Research Paper

GEOSPHERE

GEOSPHERE, v. 19, no. 3

https://doi.org/10.1130/GES02570.1

11 figures; 2 tables; 1 supplemental file

CORRESPONDENCE: Neil.Mitchell@manchester.ac.uk

CITATION: Chang, Y.-C., Mitchell, N.C., Schindlbeck-Belo, J.C., Hansteen, T.H., Freundt, A., Hübscher, C., and Quartau, R., 2023, Emplacement history of volcaniclastic turbidites around the central Azores volcanic islands: Frequencies of slope landslides and eruptions: Geosphere, v. 19, no. 3, p. 654–675, https://doi.org/10.1130/GES02570.1.

Science Editor: Andrea Hampel
Associate Editor: Valerio Acocella

Received 18 July 2022
Revision received 18 December 2022
Accepted 11 January 2023

Published online 16 March 2023

Emplacement history of volcaniclastic turbidites around the central Azores volcanic islands: Frequencies of slope landslides and eruptions

Yu-Chun Chang[1,2], Neil C. Mitchell[1], Julie C. Schindlbeck-Belo[3], Thor H. Hansteen[3], Armin Freundt[3], Christian Hübscher[4], and Rui Quartau[5,6]

[1]Department of Earth and Environmental Sciences, University of Manchester, Williamson Building, Oxford Road, Manchester M13 9PL, UK
[2]Institute of Oceanography, National Taiwan University, No. 1, Section 4, Roosevelt Road, Da'an District, Taipei City, Taiwan
[3]GEOMAR, Helmholtz Centre for Ocean Research Kiel, Wischhofstrasse 1-3, Kiel 24148, Germany
[4]Institute of Geophysics, Center for Earth System Research and Sustainability, University of Hamburg, Bundesstrasse 55, Hamburg 20146, Germany
[5]Divisão de Geologia Marinha, Instituto Hidrográfico, Rua das Trinas 49, 1249-093 Lisboa, Portugal
[6]Universidade de Lisboa, Faculdade de Ciências, Instituto Dom Luiz, 1749-016 Lisboa, Portugal

ABSTRACT

Volcanic islands export clastic material to their surrounding oceans by explosive eruptions, lava emissions, biogenic production on their shelves, and failure of their slopes, amongst other processes. This raises the question of whether geological events (in particular, eruptions and landslides) can be detected offshore and dated, and whether any relationships (for example, with climate changes) can be revealed using sediment cores. The volcanically active central Azorean islands (Faial, Pico, São Jorge, and Terceira), with their neighboring submarine basins, are potentially good candidates for such an analysis. Here, chronostratigraphies of four gravity cores collected amongst the islands are constructed based on twelve radiocarbon dates and two dates derived by geochemically correlating primary volcaniclastic turbidites with ignimbrites on Faial and Terceira Islands. Age-depth models are built from the hemipelagic intervals to estimate individual turbidite dates. Volumes of turbidites are modeled by multiplying basin areas with bed thickness, allowing for various turbidite thinning rates and directions. The volumes of landslide-generated turbidites are only comparable with the largest volumes of their adjacent upper-slope submarine landslide valleys; therefore, such turbidites in the cores likely derive from these largest landslides.

Emplacement intervals between turbidites originating from both landslides and pyroclastic density currents are found to be mostly a few thousand years. Frequencies of landslide-generated turbidites and hemipelagic sedimentation rates were both highest in the past 8 k.y. compared to preceding periods up to 50 k.y. High hemipelagic sedimentation rates are interpreted to be related to sea-level rise, allowing more shelf bioproduction and release of particles by coastal erosion. The coincident increased frequencies of submarine landslides may also be associated with the increased sediment supply from the islands, resulting in a more rapid build-up of unstable sediments on submarine slopes. Notably, the emplacement frequencies of turbidites of pyroclastic density current origins do not suggest the decreased eruption frequency toward the Holocene that has been found elsewhere.

Neil Mitchell https://orcid.org/0000-0002-6483-2450

1. INTRODUCTION

Climate changes have been suggested to modulate volcanism because of mechanical responses of volcanoes to adjustments in stresses caused by changes in loading by ice (e.g., Hall, 1982; Nakada and Yokose, 1992; Glazner et al., 1999) or, for coastal or submerged volcanoes, by seawater with sea-level fluctuation (e.g., Walcott, 1972; Wallmann et al., 1988). For instance, a lower eruption frequency has been suggested to be correlated with increased glacial loading (e.g., Jellinek et al., 2004). The reduced water loading during sea-level fall or extended sea-level lowstands may encourage decompression melting in the mantle (Walcott, 1972; Wallmann et al., 1988; Samrock et al., 2019), hence increasing volcanic activity. Satow et al. (2021) compared the past 360 k.y. of sea-level change with the tephrochronology of Santorini Volcano. Marine sediment cores revealed that ~98% of eruptive activity of Santorini Volcano occurred during periods of sea-level falls and subsequent rises. According to their 2D numerical model, the decreased hydrostatic pressure may have induced relative tensile spreading in the roof of the magma chamber, triggering dike injections and eruptions.

Large flank collapses have been reported for both intra-plate oceanic islands (e.g., the Hawaiian Islands [Moore et al., 1994], Canary Islands [Masson et al., 2002], and Cape Verde Islands [Masson et al., 2008]) and Madeira archipelago (Quartau et al., 2018) island arcs (e.g., Montserrat [Wall-Palmer et al., 2014] and Ritter Islands [Ward and Day, 2003]). Coussens et al. (2016) compiled data on 25 volcanic island landslides and found no relationship between the timing of large landslides (>0.3 km^3) and periods of rapid sea-level rise for intra-plate oceanic islands but did find a correlation for island arcs. However, the data set was small; thus, systematic changes in the timing and frequency of such events are still not well recorded or cannot

be ruled out. To address this and potential climatic modulation of eruptions, more data sets are needed of emplacement histories of volcaniclastic deposits in a variety of tectonic environments and with a variety of geomorphologies (Kutterolf et al., 2019).

The many flat-floored basins around the Azores islands lie only 10–30 km from eruptive centers and island slopes, potentially allowing the deposits arising from small events (both eruptions and slope failures) to be captured (e.g., Wall-Palmer et al., 2014). Basin-floor sediments are also of broad interest for sedimentologists and paleoseismologitsts as the "sink" that records the depositional processes and history of erosion in the "source." These source-to-sink studies have investigated how sediment in basins record processes in source areas and how individual beds are affected by basin topography (Sinclair and Cowie, 2003), varied flow rheologies (Talling, 2001), and local environments (Carlson and Grotzinger, 2001). A similar comparison of deposits with potential sources is therefore attempted here. The work here continues studies of an extensive set of samples and geophysical data collected during a RV *Meteor* cruise (Schmidt et al., 2019, 2020; Chang et al., 2022b). In this study, information from sediment cores, high-resolution multibeam bathymetric data, and seismic-reflection profiles (collected with air gun and sonar sources) were combined to work out the emplaced volumes of deposits from submarine landslides and volcanic eruptions and how they varied over time. To build chronologies, planktonic foraminifers picked from hemipelagic beds were radiocarbon-dated by accelerator mass spectrometry (AMS), and two primary tephra beds were geochemically correlated with terrestrial volcanic deposits of known dates. Volumes of turbidites in the basins were modeled by considering various distal flow thinning rates found in other similar basins elsewhere. Our main aims are to (1) estimate the volumes of volcaniclastic turbidites in the basins for comparison with volumes of potential source in the adjacent volcanic islands; (2) use a hemipelagic sediment age-depth model derived from radiocarbon ages to construct chronologies of the four cores; and (3), from their chronologies, derive emplacement frequencies for volcaniclastic turbidites produced by eruptions and landslides to see how they have changed over three periods.

2. REGIONAL SETTING

The Azores islands have developed on a broad plateau of oceanic crust thickened by excessive volcanism associated with a melting anomaly of the underlying mantle (White et al., 1976; Bonath, 1990; Gente et al., 2003; Vogt and Jung, 2004). The islands are geologically young and active (Féraud et al., 1980; Madeira and Brum da Silveira, 2003). Volcanism and tectonic activity in the Azores have been continuing during at least the Quaternary (Calvert et al., 2006; Gertisser et al., 2010; Hildenbrand et al., 2014). Moreover, eruption-fed (e.g., pyroclastic turbidite and fallout deposits) and mass transport (e.g., landslide-generated) turbidites are commonly recognized in the cores collected on the basin floors around the islands (Chang et al., 2022b), suggesting that volcanism and submarine mass transport likely occur frequently in the central Azores.

2.1 Explosive Eruptions on the Central Azores Islands

Eruptions in the central group of islands are generally moderate, i.e., low-explosivity Hawaiian to mafic phreatomagmatic eruptions (Machado et al., 1962; Madeira and Brum da Silveira, 2003; Cappello et al., 2015; Zanon and Viveiros, 2019), though explosive sub-Plinian and ignimbrite-forming eruptions have occurred on Faial and Terceira Islands (e.g., Self, 1976; Pacheco, 2001; Gertisser et al., 2010; Pimentel et al., 2015, 2021). The ignimbrite-forming eruptions were usually associated with caldera-forming or caldera-enlarging events that produced large volumes of dispersed pyroclastic fallout and pyroclastic density currents flowing tens of kilometers (e.g., Self, 1976; Gertisser et al., 2010; Pimentel et al., 2015, 2021).

Three prominent ignimbrite-forming eruptions have occurred in the past 30 k.y. The C11 eruption was the most complex and prominent eruption of Caldeira Volcano of Faial Island (Fig. 1; Pacheco, 2001; Pimentel et al., 2015). It was the largest eruption on Faial within the past 16 k.y. occurring ~1000 yr B.P. (i.e., from 1250 ± 40–1040 ± 50 yr B.P. [Madeira et al., 1995] and 980 ± 50 yr B.P. [Pacheco, 2001]), and its deposits widely blanket the island (Fig. 1). The C11 deposits have been divided into the Brejo, Inverno, and Cedros members, representing three distinct eruptive phases (Pimentel et al., 2015). According to Pimentel et al. (2015), this eruption started with a series of phreatomagmatic explosions, causing ash to fall on the NW sector of the island. The next phase (sub-Plinian) produced coarse pumice fall deposits over the north flank with most deposits dispersed in the NNW direction from the caldera. The final phase involved widespread pyroclastic density currents that reached the north and west sectors of the island. Pimentel et al. (2015) estimated the on-land tephra volume to be 0.18 km^3 (we refer to these as "bulk volumes," which are not corrected for pore space, i.e., not dense rock equivalent). The total tephra volume including submarine deposits was estimated by them to be >0.22 km^3 using empirical methods of Sulpizio (2005) combined with those of Fierstein and Nathenson (1992).

Ignimbrites on Terceira Island constitute a significant portion of the island stratigraphy. At least seven ignimbrite sequences were emplaced between ca. 86 and 25 cal k.y. B.P. (Calvert et al., 2006; Gertisser et al., 2010; Pimentel et al., 2021). The most recent Lajes-Angra Ignimbrite Formation originated from eruptions of Pico Alto Volcano (Fig. 1). Two ignimbrites were initially interpreted by Self (1976) as resulting from two eruptions of Pico Alto Volcano—the Angra and Lajes ignimbrite-forming eruptions. Although the Angra and Lajes ignimbrites have similar whole-rock major-element compositions and mineral assemblages, their whole-rock trace-element and volcanic glass compositions differ considerably (Pimentel et al., 2021). Moreover, the Angra Ignimbrite is only exposed in a narrow valley in the southern part of the island. The Lajes Ignimbrite, in contrast, is widely exposed in the southern, middle, and northern parts of Terceira (Fig. 1). Radiocarbon dates of

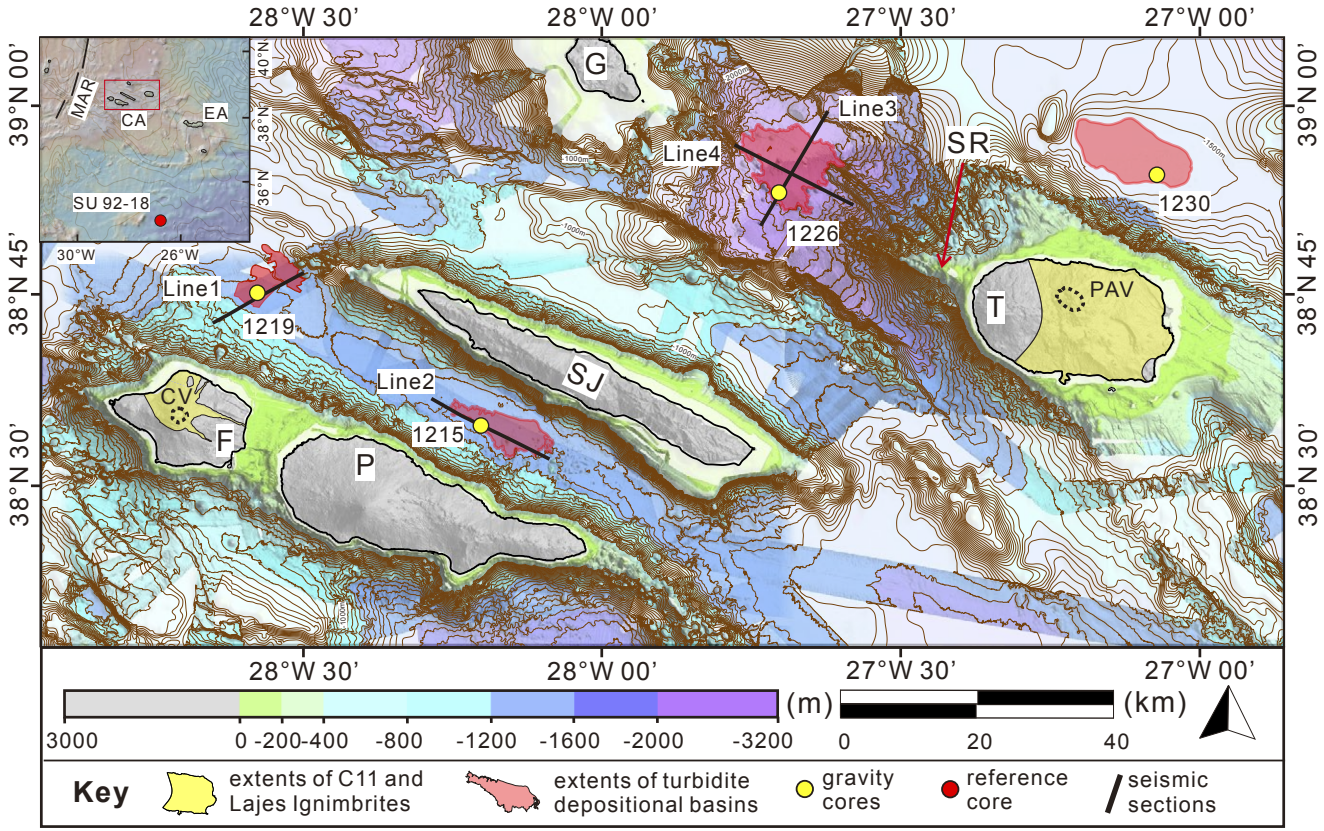

Figure 1. Bathymetry of the central Azores Islands contoured every 50 m from 500 to 3200 m. High-resolution multibeam echo-sounder data are shown in bold colors as in color bar. Bathymetry in faint colors is from the Global Multi-Resolution Topography Synthesis (Ryan et al., 2009). Light-gray areas represent the islands of Faial, Pico, São Jorge, Terceira, and Graciosa (F, P, SJ, T, and G, respectively). SR is submarine Serreta Ridge. Black dashed lines outline the calderas of Caldeira Volcano (CV) and Pico Alto Volcano (PAV). Yellow areas show extents of volcanic deposits on Faial (from the C11 eruption) and Terceira (Lajes eruption), which include volcanic ash and ignimbrites. Yellow circles locate the gravity cores summarized in Figure 2. Black lines (1–4) locate the seismic sections in Figure 8. Salmon-filled polygons represent extents of turbidite depositional basins identified from depth contours and seismic-reflection data. Inset locates study area (rectangle outlined in red) and reference core site (red circle). CA, EA, and MAR represent the central Azores, eastern Azores islands, and Mid-Atlantic Ridge, respectively.

charcoal below and within the Lajes and Angra ignimbrites (Calvert et al., 2006; Gertisser et al., 2010), calibrated with the IntCal20 calibration curve (Reimer et al., 2020), suggest the Angra Ignimbrite was emplaced 25.3–28.1 cal k.y. B.P. (Gertisser et al., 2010) and the Lajes Ignimbrite 23.0–28.8 cal k.y. B.P. (Gertisser et al., 2010) or 25.2–25.9 cal k.y. B.P. (Calvert et al., 2006). Their juvenile clasts are characterized by coarse porphyritic pumices, including light-gray comenditic trachyte pumice and dark-gray or black scoriae, but the black dense clasts occur exclusively in the Lajes Ignimbrite (Pimentel et al., 2021). The on-land bulk volumes of the Angra Ignimbrite and Lajes Ignimbrite were estimated to be 0.08 km^3 and 0.59 km^3, respectively (Pimentel et al., 2021).

2.2 Volcanism-Associated Sediment Gravity Flows as Turbidite Sources

Deposits from pyroclastic density currents and fallout have been recognized on the Azores islands (e.g., Cole et al., 2001; Pacheco, 2001) and identified in our four sediment cores near the islands (Chang et al., 2022b; Fig. 2). Hawaiian to mildly explosive

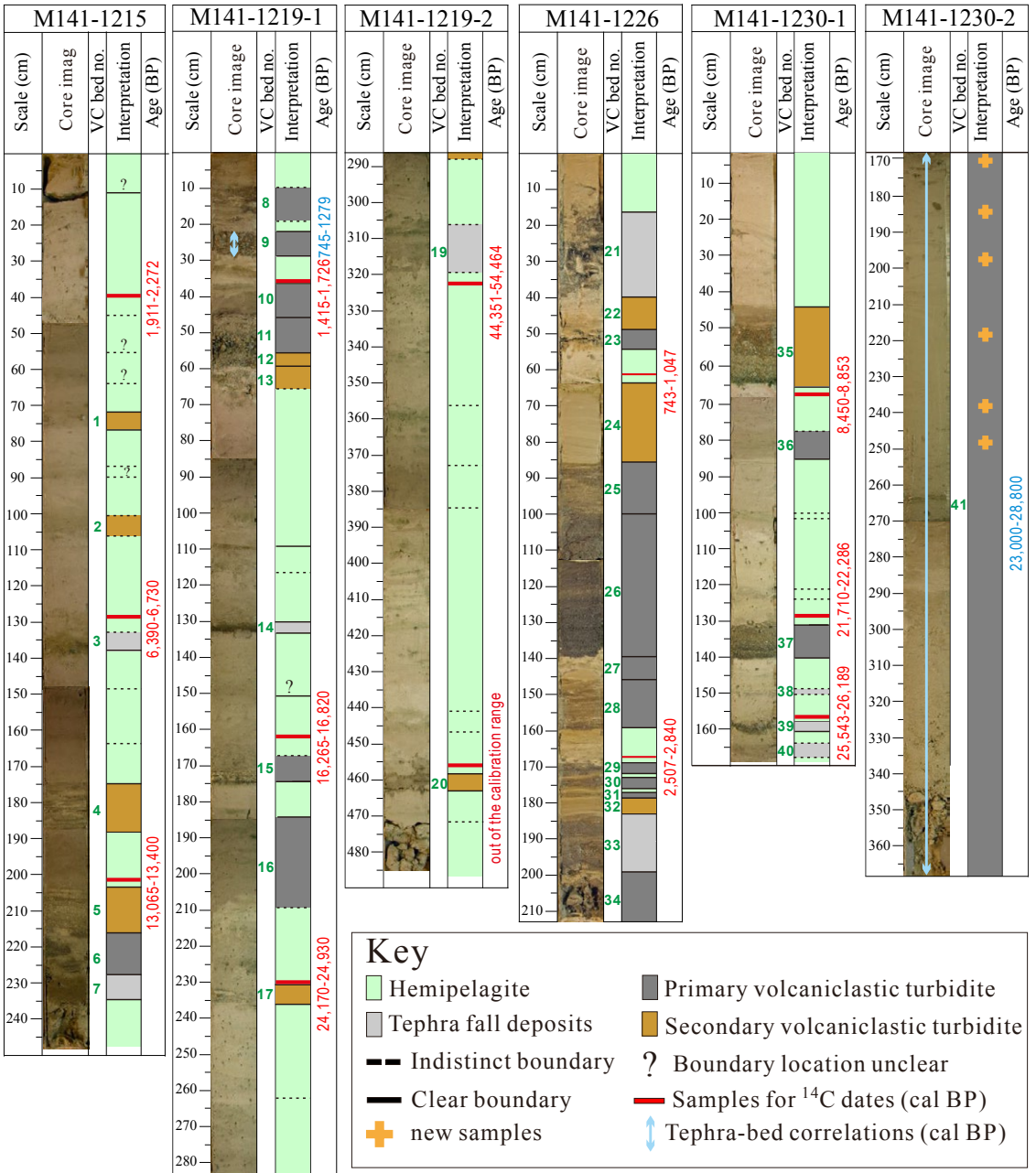

Figure 2. Summary of cores taken from the sites located in Figure 1. Red values are calendar ages derived from the ^{14}C dates. Photographic scans and interpreted deposit emplacement mechanisms are simplified from Chang et al. (2021). Light-blue, double-headed arrows locate tephra correlated with erupted unit on land, with corresponding 95% age intervals (Pimentel et al., 2015, 2021). Numbering of the volcaniclastic (VC) beds in the third columns (green text) corresponds with Table 2, which lists their estimated calendar ages. Numbers 9 and 41 locate samples for geochemical correlation of tephra.

Strombolian eruptions have likely occurred frequently (e.g., many times over the period of human habitation; Weston, 1964; Madeira and Brum da Silveira, 2003); so there is also a potential for submarine-emplaced lava flows to initiate sediment flows either due to the flow disintegration arising from rapid transportation on steep slopes (Bergh and Gudmunder, 1991) or flow-front failures caused by piling up of lava fragments (Lodato et al., 2007; Mitchell et al., 2008; Quartau et al., 2015). Collapses due to slope overloading and oversteepening (Mitchell et al., 2012; Costa et al., 2014, 2015) result in large-scale mass movements, which can evolve downslope into sediment gravity flows.

Figure 2 shows 41 volcaniclastic-rich beds found in the sediment cores located in Figure 1. These are updated from the identifications of Chang et al. (2021) as described later in this article. The beds include nine pyroclastic fallout beds and 33 volcaniclastic turbidites. The turbidites were further classified into primary volcaniclastic turbidites (PVTs) and secondary volcaniclastic turbidites (SVTs). PVTs originate directly from pyroclastic flows where transport occurs without an intervening stage of deposition and remobilization. SVTs instead likely involve events unrelated to volcanic activity such as deposits remobilized by slope failure. SVTs are separated from PVTs by common shelf biogenic material (carbonates), rounded volcanic particles, low proportions of glass shards, commonly heterogeneous glass shard compositions, and larger organic contents. Two-thirds of the turbidites identified in the cores are PVTs. Their thicknesses are typically 0.05–0.15 m, though two PVTs of 0.4 and 2 m were found. Although the PVTs were likely created by pyroclastic density currents from eruptions of the adjacent islands, core 1226 located within the Terceira Rift may have received PVTs from submarine eruptions on the Serreta Ridge, which is volcanically active (Gaspar et al., 2003; Madureira et al., 2017; Casas et al., 2018; Romer et al., 2019).

2.3 Other Sources of Sediment Gravity Flows

Processes that have been suggested to generate sediment gravity flows on submarine slopes elsewhere also occur in the Azores. For instance, more than a thousand submarine landslide valleys have been identified along the upper slopes of four islands in the central Azores (Chang et al., 2021). Downslope mass movements (landslides) may transform into turbulent sediment gravity flows if the mass disintegrates during movement (e.g., Nisbet and Piper, 1998; Piper et al., 2007). Landslides in the Azores potentially can be induced by frequent earthquakes (Gaspar et al., 2015). High ocean surface waves, which predominantly approach the islands from the NW, have been suggested to be responsible for more frequent submarine sediment gravity flows on the windward sides of islands indicated by more common sediment waves on the seabed on that side (Chang et al., 2022a). Such a higher frequency could arise from an increased sediment flux from wave erosion (e.g., Quartau et al., 2012; Zhao et al., 2020) supplying unconsolidated sediment to upper slopes, where it is prone to failure, or enhanced wave-agitated turbulent flows (e.g., Normandeau et al., 2020; Porcile et al., 2020).

In the investigated cores (Fig. 2), one-third of the turbidites are SVTs and hence involved some reworking of bed material, such as evidenced by the fragments of carbonate of shelf origin and higher organic contents. The lower abundance of SVTs compared with PVTs suggests either that volcanic eruptions in the Azores are more frequent than slope failures or that sediment gravity flows generated by slope failures have not all reached the basin floors (Chang et al., 2022a). The SVTs thicknesses are similar to PVT thicknesses, but no SVTs thicker than 0.2 m have been found.

3. MATERIALS AND METHODS

3.1 Sediment Cores and Sample Collections

The four gravity cores were collected during RV *Meteor* cruise M141/1 in 2017 (Hansteen et al., 2017). These cores were sampled for radiocarbon accelerator mass spectrometry (AMS) analysis (red bars) and volcanic glass compositional analysis (orange crosses) at the stratigraphic levels shown in Figure 2.

3.1.1 Samples for Radiocarbon Dating

For radiocarbon dating, 13 samples were selected mostly in hemipelagic beds immediately overlying turbidites and tephra beds (Fig. 2). For those beds with gradational or bioturbated boundaries, samples were collected where hemipelagite and turbidite are in equal proportions. That proximity should allow reasonable estimates of the turbidite ages to be determined. Pretreatment of samples included sediment disaggregation in 10 wt% sodium hexametaphosphate, ultrasonic bathing, rinsing, and wet sieving (Hajdas, 2008; Brock et al., 2010). Approximately 10 mg of planktonic foraminifers showing little sign of damage or alteration were hand-picked under a high-power dissecting microscope (e.g., Fig. 3). *Globigerina bulloides* and *Globigerinoides ruber* species were mainly selected due to their abundance. Although we prioritized mono-planktonic species to reduce the Barker effect (i.e., an effect causing radiocarbon age biases due to the differential effect of partial dissolution and subsequent fragmentation of shells [e.g., Ausín et al., 2019]), other surface-dwelling planktonic species (e.g., *Globigerinella siphonifera* and *Globigerinoides sacculifer* shown in Figs. 3C and 3D) were still sometimes included where abundance of the preferred species was low.

The AMS analysis was conducted by the National Environmental Isotope Facility (NEIF) radiocarbon laboratory at the Scottish Universities Environmental Research Centre (SUERC). Samples were acid-leached to remove external carbon contamination on outer shell surfaces (Hajdas, 2008; Brock et al., 2010) and then converted into pure and condensed carbon (Povinec et al., 2009) suitable for AMS analysis. Ratios of $^{13}C/^{12}C$ were measured by isotope ratio mass spectrometry (IRMS), and the $\delta^{13}C$ values (deviation from reference $^{13}C/^{12}C$) were calculated relative to the Vienna Pee Dee Belemnite (VPDB) standards. Contents of ^{14}C were then corrected for fractionation by normalizing $\delta^{13}C$ to –25‰. The conventional radiocarbon age (yr B.P.) with ±1σ confidence ranges are shown in Table 1.

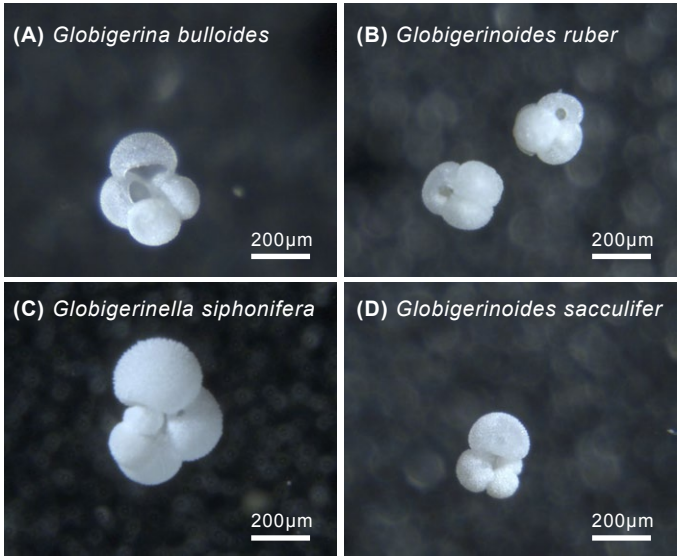

Figure 3. Selected photos of planktonic foraminifera species from the samples used for radiocarbon dating. (A) *Globigerina bulloides*. (B) *Globigerinoides ruber*. (C) *Globigerinella siphonifera*. (D) *Globigerinoides sacculifer*. The species in (A) and (B) were the main ones selected for ^{14}C dating in this study. Note glassy surface textures suggesting lack of alteration.

3.1.2 Radiocarbon Age Calibration and Age-Depth Modeling

To correct for varying production rates of radiocarbon through time (Lal and Peters, 1967), radiocarbon ages were converted to calendar ages using Marine20 (Heaton et al., 2020), a marine-specific calibration curve that corrects for the global average of marine reservoir effect (MRE) for non-polar areas. Correcting for a local MRE (i.e., deviation from the global curve or ΔR) is difficult around the Azores due to the lack of established values and appropriate materials for assessment (e.g., Ascough et al., 2005). Comparing global ΔR variations (Reimer and Reimer, 2001) with oceanic circulation in Ascough et al. (2005), however, ΔR around the Azores is probably between –51 and +14 yr. Such corrections are small compared with age differences between samples reported in the text below; therefore, variations in ΔR are ignored in this study.

Volcaniclastic bed thicknesses were extracted from each core to build hemipelagic sediment age-depth models. How hemipelagic sedimentation rates have varied over time in detail amongst the Azores islands is uncertain. These sediments contain a poorly quantified but likely important volcaniclastic component (fine particles from coastal erosion and ash from eruptions). Because other contributions from slope failure, cliff failure, fluvial outwash during storms, and biogenic production varying with nutrient availability and climate are all episodic, we suspect that sedimentation rates have varied strongly between our age constraints. Since the hemipelagic sedimentation process is therefore uncertain, we have chosen not to use Bayesian methods for age-depth modeling (e.g., Ramsey, 2008; Blaauw, 2010). We have instead modeled deposition using simple linear age variations between dates. To be accurate, such age-depth modeling relies on two assumptions, which we

TABLE 1. INFORMATION ON MICROFOSSIL SAMPLES AND RADIOCARBON DATING RESULTS

Publication code	Sample ID	Sample depth (bsf cm)	Sample weight (mg)	Boundary	Dominant dated species	Conventional radiocarbon age (±1σ, yr B.P.)	$\delta^{13}C$ VPDB (‰)	Calendar age (cal yr B.P.)	Best calendar age estimates (yr B.P.)
SUERC-100215	1215-1	39–40	10.6	Gradational	*G. bulloides* and *G. ruber*	2570 ± 35	0.0	1911–2272	2070
SUERC-100216	1215-4	128–129	10.2	Gradational	*G. ruber*	6315 ± 38	–0.3	6390–6730	6559
SUERC-100217	1215-7	201–202	10.5	Gradational	*G. bulloides*	11,901 ± 52	–1.1	13,065–13,400	13,220
SUERC-100218	1219-1	35–36	10.7	Gradational	*G. bulloides* and *G. ruber*	2,168 ± 35	1.0	1415–1726	1582
SUERC-100219	1219-3	162.5–163.5	10.3	Gradational	*G. bulloides*	14,349 ± 57	–0.9	16,265–16,820	16,535
SUERC-100223	1219-5	229.5–230.5	10.2	Gradational	*G. bulloides*	21,252 ± 116	–0.6	24,170–24,930	24,543
SUERC-100224	1219-7	322–323	10.4	Sharp	*G. bulloides*	45,384 ± 2281	–0.6	44,351–54,564	46,992
SUERC-100225	1219-8	456.5–457.5	10.6	Gradational	*G. bulloides*	>46,665	–0.9	Out of range	Out of range
SUERC-100226	1226-3	61–61.5	7.1	Gradational	Mixture of four species	1512 ± 37	–1.0	743–1047	894
SUERC-100227	1226-8	167–167.5	8.2	Gradational	Mixture of four species	3064 ± 37	–1.1	2507–2840	2691
SUERC-100228	1230-2	67–68	10.7	Sharp	*G. siphonifera* and *G. ruber*	8301 ± 37	0.5	8450–8853	8636
SUERC-100229	1230-4	128–129	10.7	Sharp	*G. bulloides* and *G. ruber*	18,924 ± 89	–0.7	21,710–22,286	22,006
SUERC-100233	1230-6	156–157	10.5	Sharp	*G. bulloides*	22,473 ± 134	–1.2	25,543–26,189	25,837

Notes: bsf—below sea floor; VPDB—Vienna Pee Dee Belemnite.

return to later: (1) no change in hemipelagic sedimentation rate between dates (e.g., Milkert et al., 1996; Lebreiro et al., 2009; Clare et al., 2015; Allin et al., 2016); and (2) negligible surficial deposits have been removed by turbidity currents as they accumulated by instantaneous depositional processes (e.g., Weaver and Thomson, 1993; Thomson and Weaver, 1994; Gutierrez-Pastor et al., 2009; Gràcia et al., 2010). Individual estimated calendar ages of each volcaniclastic-rich bed are calculated from the linear interpolation between calendar ages of dated samples. In practice, the sediment only at the dated samples can be unequivocally assigned ages with uncertainties. Nevertheless, some dates lie close to the 8 and 20 ka boundaries between sediment groups in these cores. This effectively allows us to assign parts of the cores to different groups reasonably reliably (e.g., 8 ka for cores 1215 and 1230 and 20 ka for cores 1219 and 1230).

Hemipelagic sedimentation rates were calculated by dividing the calendar age differences between samples by the cumulative thickness of hemipelagic beds within them. Hemipelagic sedimentation rates were then found for discrete age intervals representing the different periods of sea-level change (0–8, 8–20, and 20–50 k.y.) by dividing the cumulative hemipelagic thicknesses by their time spans. Rates for those core intervals that do not entirely extend over a full age interval were computed by dividing the hemipelagic thickness by their reduced durations. A more regional hemipelagic sedimentation rate curve was then computed by averaging the individual interval-averaged hemipelagic sedimentation rates of the four cores. The same calculation was also used to derive individual core and total interval-averaged frequencies of PVTs and SVTs within the selected date intervals after assigning dates to individual beds using the hemipelagic thicknesses.

3.1.3 Samples for Sediment Core Reinterpretation and Tephrostratigraphic Correlations

The classification of bed types of Chang et al. (2021) shown in Figure 2 was updated in the light of data from six volcaniclastic samples (crosses in Fig. 2) from core 1230 at depths 168–262 cm below sea floor (bsf). Sample pretreatment and analytical procedures followed those of Chang et al. (2021). Backscattered-electron images of whole samples were captured by JEOL JXA 8200 wavelength dispersive electron microprobe (EMP). Major elements were measured on volcanic glass shards by EMP at GEOMAR Helmholtz-Centre for Ocean Research Kiel following procedures described in Kutterolf et al. (2011).

Primary volcaniclastic turbidites (PVTs) in cores 1219 (22–29 cm bsf) and 1230 (168–368 cm bsf) were correlated with ignimbrites on adjacent islands. Correlations followed the established methods of Kutterolf et al. (2008) and Schindlbeck et al. (2016, 2018) by comparing the major geochemical elements of volcanic glass shards from marine tephras with those of island samples, while their stratigraphic positions were validated using the age-depth model based on the radiocarbon dates. Mineral assemblage data and sedimentary features were also considered if they were available. The geochemical correlations are constrained by overlaps of multiple elements.

3.2 Marine Geophysical Data

Multibeam bathymetric data were collected in four surveys at resolutions ranging from 0.5 to 1 m in the shallowest 100 m to 20–50 m at 2000 m depth. The combined data set broadly covers the submarine part of the central group of the Azores (Fig. 1). The RV *Arquipélago* survey in 2003 investigated the submarine parts of Faial, Pico, and São Jorge islands (Mitchell et al., 2008). The *l'Atalante* survey (EUROFLEETS cruise "Features of Azores and Italian Volcanic Islands" [FAIVI]) in 2011 investigated predominantly the shelf and slopes of Terceira Island (Chiocci et al., 2013; Quartau et al., 2014; Casalbore et al., 2015). Though mainly investigating the area around São Miguel Island, the two RV *Meteor* surveys in 2009 (cruise M79/2; Hübscher, 2013) and 2015 (cruise M113/1; Hübscher et al., 2016) also partly covered the central group, in particular the basin between submarine Serreta Ridge and Graciosa Island.

Two-dimensional (2D), multichannel, seismic-reflection profiles were collected during cruise M113 (Hübscher et al., 2016) using two GI guns as a source (chamber volumes of 45 and 105 in^3). Signals were recorded with a 144-channel acquisition system. The main seismic processing steps were editing, common mid-point binning, bandpass filtering over the range 10/20–300/400 Hz, gain, stacking, time migration, and fx deconvolution. Processing is described further by Hübscher and Gohl (2014).

During M113, sediment profiler data were also acquired using a hull-mounted Parasound system (Atlas Hydrographics) simultaneously with the multichannel seismic data. This system operates by emitting two pulses with high primary frequencies (18 kHz and 22 kHz), which combined nonlinearly in the water to produce a signal at their difference frequency of 4 kHz. The beams produced by the high primary frequencies form cones of <4° width, resulting in data without diffraction hyperbolae. Hence, Parasound data have high vertical and lateral resolution. Processing applied to the Parasound data included amplitude amplification and frequency filtering. Depths below seabed have been derived from the Parasound data assuming a water velocity of 1500 m/s.

3.3 Turbidite Volume Modeling

If turbidites form simple flat-lying deposits of uniform thickness within basins, turbidite volumes can be estimated by multiplying the basin area with the turbidite thicknesses found in the cores. For such calculations, the area of each basin floor can be delimited using a closed bathymetric contour line (Fig. 1) located at the base of slope or tectonic structures revealed by the seismic sections and encompassing the core site. This approach makes the implicit assumption that turbidity currents, which are typically channeled on the slopes, are sufficiently mobile to spread out across the entire flat basin floor with uniform thickness.

To allow for bed distal thinning, the results of more detailed analysis of turbidite geometries in similar basins (e.g., Liu et al., 2018) were used. Liu et al. (2018) classified thinning as occurring at

low (3%–15%/km) and high (40%–65%/km) rates. Representing the rate with K (1/km), the rate of change is:

$$dT / dx = -KT, \quad (1)$$

where T is bed thickness, and x is distance. Integrating from a fixed reference point chosen at the origin (x = 0 km) suggests:

$$T = T_0 = \exp(-Kx), \quad (2)$$

where T_0 is the bed thickness at the reference position x = 0 km. To implement the exponential model, the delimited basins (Fig. 4A) were idealized as rectangles of areas equal to the basins (Fig. 4B). The length and width of each rectangle were adjusted to represent approximately the dimensions of each basin. Although turbidity currents potentially entered each basin from any side, we identified those sides that were closest to the most likely sources (for example, PVTs were most likely produced by eruptions of adjacent islands and SVTs by failure of adjacent steep slopes). Volumes calculated with different source directions then represent the effect of this uncertainty. Where a core site is distal to the assumed source, the calculation resulted in volumes that are larger than when no thinning was assumed. In contrast, core sites close to the source resulted in smaller volumes than when no thinning is assumed.

For each chosen source direction, volumes were estimated in practice by numerically integrating T in a series of 1 km steps over the direction in which the flows are assumed to have entered the basin and multiplying by rectangle width. Thinning rates of 9%, 30.75%, and 52.5%/km were used, encompassing the appropriate rates of Liu et al. (2018). Best estimates of individual turbidite volumes were derived using the most likely sediment entry direction and thinning rates suggested from seismic-reflection data.

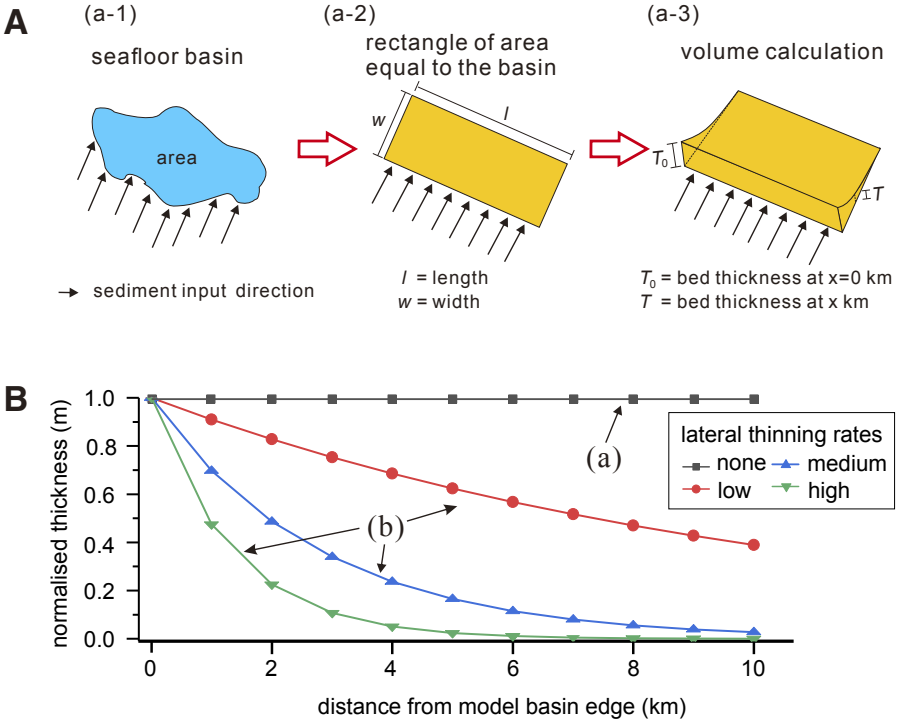

Figure 4. Conceptual elements of geometry used in calculation of turbidite volume, which attempts to account for varied degrees of deposit confinement and distal thinning rate. (A) Concept of turbidite volume calculation. (B) Turbidite thickness change from model basin edge, encompassing four thinning rates. Bed thicknesses are normalized to 1 m at 0 km distance in this illustration; however, true thicknesses are used in the analyses.

4. RESULTS

4.1 Stratigraphy of the Sediment Cores

The core stratigraphy that we established previously (Chang et al. 2021) was improved and extended by: (1) reinterpreting one segment of hemipelagic beds in core 1230 as a primary volcaniclastic turbidite; (2) geochemically correlating two volcaniclastic beds with well-dated ignimbrites on Faial and Terceira Islands; and (3) incorporating the 12 new radiocarbon dates.

4.1.1 Bed Reinterpretation

Chang et al. (2021) originally interpreted the 168–262 cm bsf section of core 1230 as hemipelagic sediment because this fine-grained section lacked tractional structures. However, visual inspection and chemical analyses by EMP of six additional samples (located in Fig. 2) have led us to reinterpret the section. Selected backscattered-electron images of 63–125 µm fraction from core 1230 at 168–170 cm bsf and 248–252 cm bsf revealed predominant volcanic glass shards and some biogenic matter and lithics (Figs. 5A and 5B), which are similar to samples at 262–368 cm bsf (Chang et al., 2021). Besides minor outliers, major elements of four samples from the segment clustered closely (Figs. 5C and 5D). The consistency of the volcanic

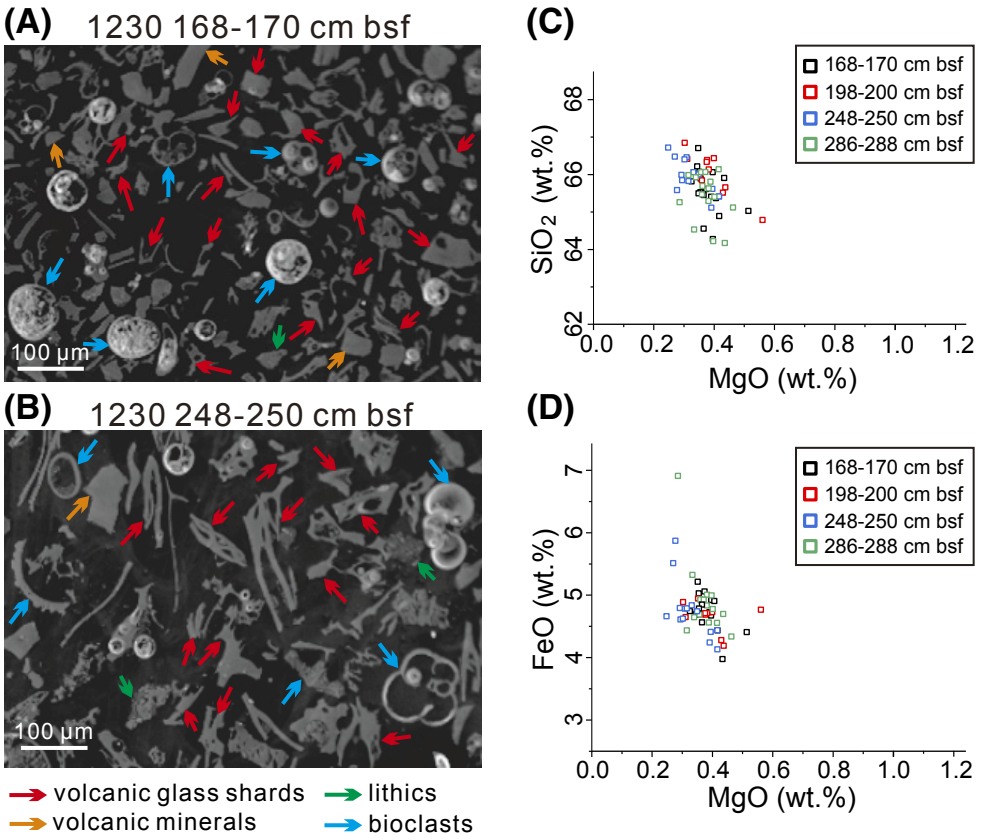

Figure 5. Data from samples of primary volcaniclastic beds in core 1230. Backscattered-electron microscope images in (A) and (B) are from the core depths marked above each image. Red, orange, blue, and green arrows mark interpreted volcanic glass shards, volcanic minerals, bioclasts, and lithics, respectively. Major-element compositions in (C) and (D) measured on glass shards taken from the core depths shown in the graph keys. Three outliers out of >80 analyses were excluded from the graphs. bsf—below sea floor.

glass geochemical compositions across the interval suggests that the upper boundary of the thick turbidite previously placed at 262 cm bsf should be elevated to 168 cm bsf. The geochemical data for these six samples are provided in Table S1[1].

[1]Supplemental Material. Table S1: Geochemical data for six samples. Please visit https://doi.org/10.1130/GEOS.S.21980360 to access the supplemental material, and contact editing@geosociety.org with any questions.

4.1.2 Tephrostratigraphic Correlations

Evidence suggests that samples of core 1219 at 22–29 cm bsf and 1230 at 168–368 cm bsf correlate with ignimbrites on Faial (C11) and Terceira Islands (Lajes), respectively: (1) Multiple major elements (MgO, SiO_2, FeO, CaO, and TiO_2) derived from the groundmass glasses of the land samples overlap with those of the core samples (Fig. 6). (2) The elongated and stretched light-gray pumiceous glass shard (e.g., Figs. 5A and 5B) both dominate the bed of core 1230 and the Lajes ignimbrite (Pimentel et al., 2021). Most mineral assemblages (e.g., anorthoclase, clinopyroxene, and olivine phenocrysts) in core 1230 (Chang et al., 2021) are also similar to those described in the Lajes ignimbrite (Pimentel et al., 2021). (3) The stratigraphic positions and dates of emplacement of these two ignimbrites (Calvert et al., 2006; Gertisser et al., 2010) are compatible with our hemipelagic age-depth models (see section 4.2). The ranges of radiocarbon dates of charcoal below and within the ignimbrites calibrated with IntCal 20 are 745–1279 cal yr B.P. for the C11 eruption and 23,000–28,800 cal yr B.P. for the Angra-Lajes eruption (Pimentel et al., 2021). Our age-depth model suggests 974 cal yr B.P. for the C11 bed and 27,179 cal yr B.P. for the Lajes bed. These dates are well constrained by ^{14}C dates adjacent to the beds (1415–1726 cal yr B.P. in core 1219 and 25,543–26,189 cal yr B.P. in core 1230). As mentioned earlier, we assign this bed to the Lajes ignimbrite given that the Angra ignimbrite only outcrops in a valley on the south of the island (opposite the core site).

4.1.3 Radiocarbon Dates and Age-Depth Modeling

The calendar dates and two dates of the ignimbrites correlated with volcaniclastic beds are shown in Figures 2 and 7. Most calendar dates had narrow uncertainty ranges (~350 yr) except the fourth sample in core 1219 (~10,000 yr), where radiocarbon concentration was low. The $\delta^{13}C$ values (1.0 and –1.0) are typical of marine foraminifera, also indicating low terrestrial contamination. The dates progressively increase down each core with no age reversals. The radiocarbon dates and associated data are listed in Table 1.

4.1.4 Sedimentation History

Figure 7 shows the combined results derived from the 12 radiocarbon and two correlated

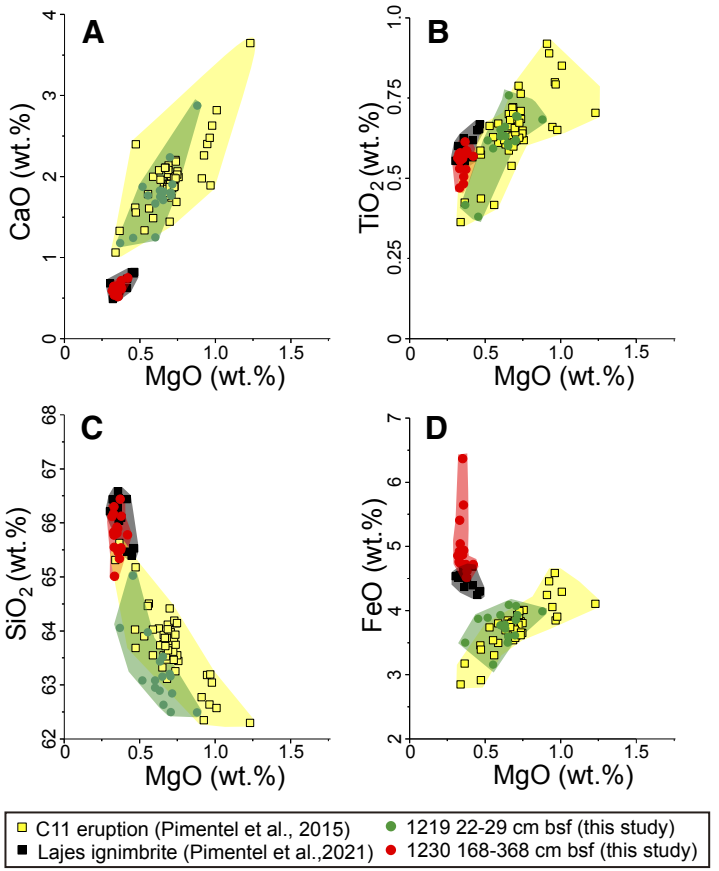

Figure 6. Comparison of major-element compositions of two well-dated ignimbrites on land with those of volcanic glass shards in the sediment cores. Panels (A–D) compare data from core 1219 (22–29 cm below sea floor [bsf]) with products of the Faial C11 eruption (Pimentel et al., 2015) and data from core 1230 (168–368 cm bsf) with products of the Terceira Lajes eruption (Pimentel et al., 2021).

ignimbrites. Although these 14 dates leave some temporal variations unresolved, they are sufficient to group the deposits by date so that changes between deposit groups can be explored. For these group periods, we use inflections in the sea-level curve of Spratt and Lisiecki (2016); their curve contains clearly different regimes of highstand (0–8 k.y.), transgression (8–20 k.y.) and regression (20–50 k.y.). Stratigraphy within core 1219 is older than the oldest dateable radiocarbon date (~1.5 m of hemipelagics). One SVT within that interval was dated by extrapolation using the hemipelagic sedimentation rate from the overlying two radiocarbon dates.

All dates progressively increase with depth with no major change of trend that might indicate sediment abruptly removed by erosion (eroded intervals are not resolved) in each of the four hemipelagic sediment age-depth models shown in Figure 7A (black lines). They mostly steepen into the Holocene, in particular, where dates close to 8 ka are available for cores 1215 and 1230. This is reflected in greater average hemipelagic sedimentation rates shown by the pink bars in Figure 7A, which increase from ~4 cm/k.y. in the regression period to ~11 cm/k.y. in the highstand period. Focusing on the better constrained stratigraphy after the regression period, sedimentation rates increased from transgression to highstand periods by nearly a factor of two. These rates are all higher than the average open-ocean sedimentation rate at site SU92-18 (3.5 cm/k.y.; Vlag et al., 2004).

The interval-averaged frequencies of emplacements of primary and secondary volcaniclastic turbidites (PVTs and SVTs, respectively) are shown at the top of Figure 7A (light-tone and dark-tone olive-green bars, respectively). Return periods of both types of turbidites are >1 k.y. The frequencies of PVT and SVT emplacements were both higher during the transgression and particularly during the highstand period compared to the preceding regression period (Fig. 7A). Relative to frequencies during the regression period, PVT emplacements increased by a factor of 2.5 during transgression and by a factor of 6 during the highstand. SVT emplacements increased by factors of 4.5 and 7.5 over the corresponding periods.

Examining the records from individual cores (Fig. 7C), along with the locations of age constraints (Fig. 2), these frequencies vary among sites. While emplacement frequencies of all turbidite types in cores 1230 and 1215 were comparable between transgression and highstand, in core 1219, frequencies increased into the highstand period. Although no date was recorded in 1219 close to 8 ka, the uppermost six turbidites were well constrained by the 1415–1726 cal yr B.P. date. The PVT frequencies in cores 1215 and 1230 slightly decreased toward the highstand period, whereas the frequency in core 1219 increased. Although core 1226 did not penetrate sediment older than 8 ka, its PVT frequency was higher than the other cores, and that high frequency is well constrained (Fig. 2). SVT frequencies of cores 1215, 1219, and 1230 all consistently increased into the highstand period.

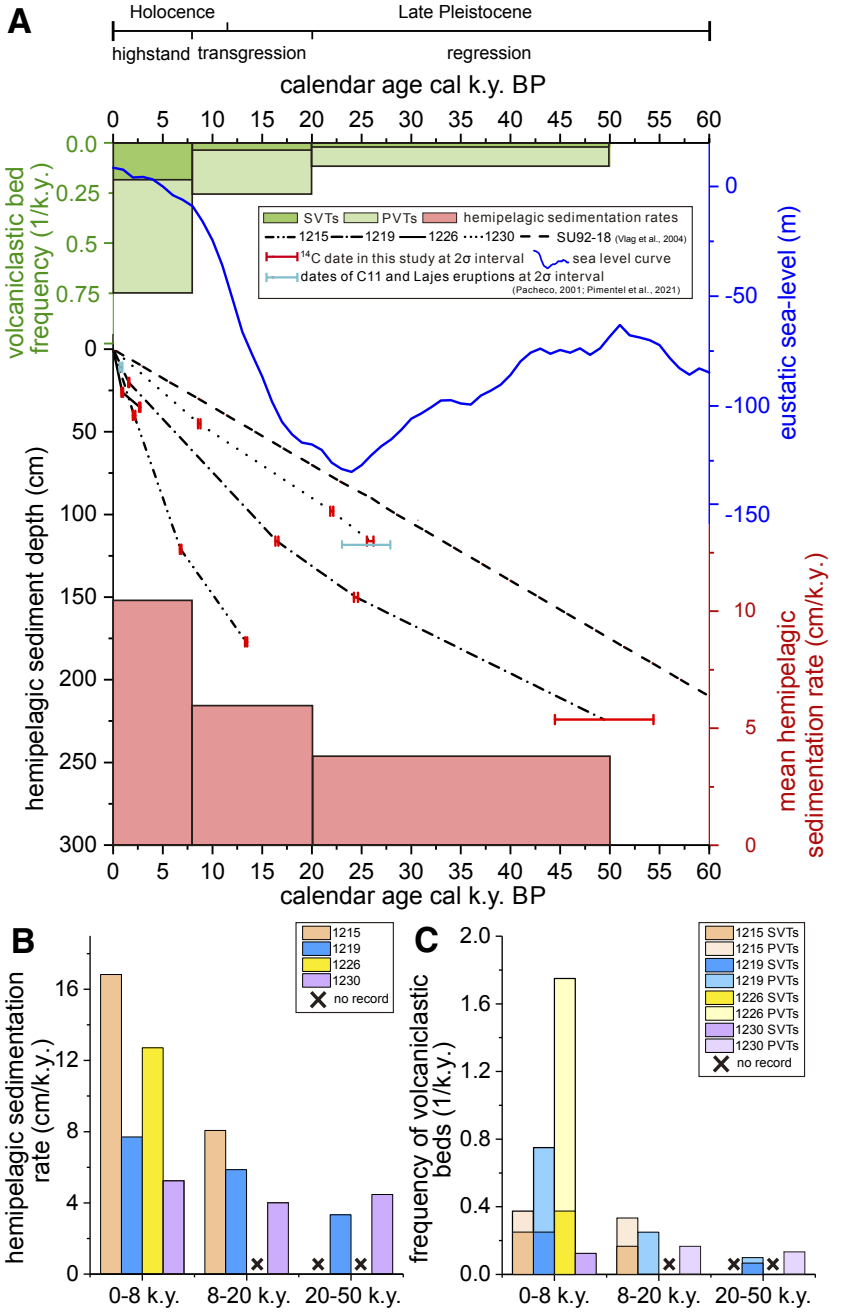

Figure 7. Sediment deposition history in the cores based on the ^{14}C dating and two correlated ignimbrites. (A) Black lines (scale to lower left) are hemipelagic age-depth models for the cores based on calendar age intervals (red horizontal bars represent the 95% confidence level). Double-dashed line is the 3.5 cm/k.y. depth-averaged deep-sea hemipelagic sedimentation rate of Vlag et al. (2004) for a site located in inset to Figure 1. Blue curve is eustatic sea-level variation of Spratt and Lisiecki (2016). Olive-green bars are the interval-averaged frequencies of volcaniclastic turbidites for all cores combined. Pink bars are interval-averaged hemipelagic sedimentation rates that have been averaged between the four cores where stratigraphy is present. (B) Interval-averaged hemipelagic sedimentation rates of individual cores. (C) Interval-averaged frequencies of volcaniclastic turbidites of individual cores. Black crosses in (B) and (C) mark where cores did not penetrate to the age range shown. PVTs—primary volcaniclastic turbidites, SVTs—secondary volcaniclastic turbidites.

4.2 Turbidite Volume Modeling Results

Seismic sections (Figs. 8B–8D) and bathymetric data (Fig. 9A) show that the sites of cores 1215, 1226, and 1230 are located within closed-contour depressions and/or surrounded by tectonic structures (e.g., faults); thus, their basin floors are well constrained. In contrast, core 1219 was collected from the lower slope of Faial Island (Fig. 8A). For that site, we approximated the depositional basin length as extending from a small escarpment upslope to the edge of a graben downslope (Fig. 8A) and the basin width as the graben length. The rectangles modeling basin areas shown in Figures 8A to 8D have areas of 3.9×10^7–1.1×10^8 m^2.

The in situ distal thinning of beds was assessed using Parasound data collected perpendicular to suspected sediment input directions (Figs. 8F and 8G). In Figure 8F (northwest of Terceira), an interval encompassing a transparent section (a possible mass-transport deposit bracketed by red bars) tapers westward from 3.56 to 1.4 m thickness over a distance of 2.83 km, suggesting a thinning rate of 33%/km, close to the moderate thinning rate of Liu et al. (2018). As such a thinning rate is most appropriate for the thicker beds in the cores, using it may introduce some bias in the results for the thinner beds, but we are primarily interested in correlating these beds with large features (landslide valley

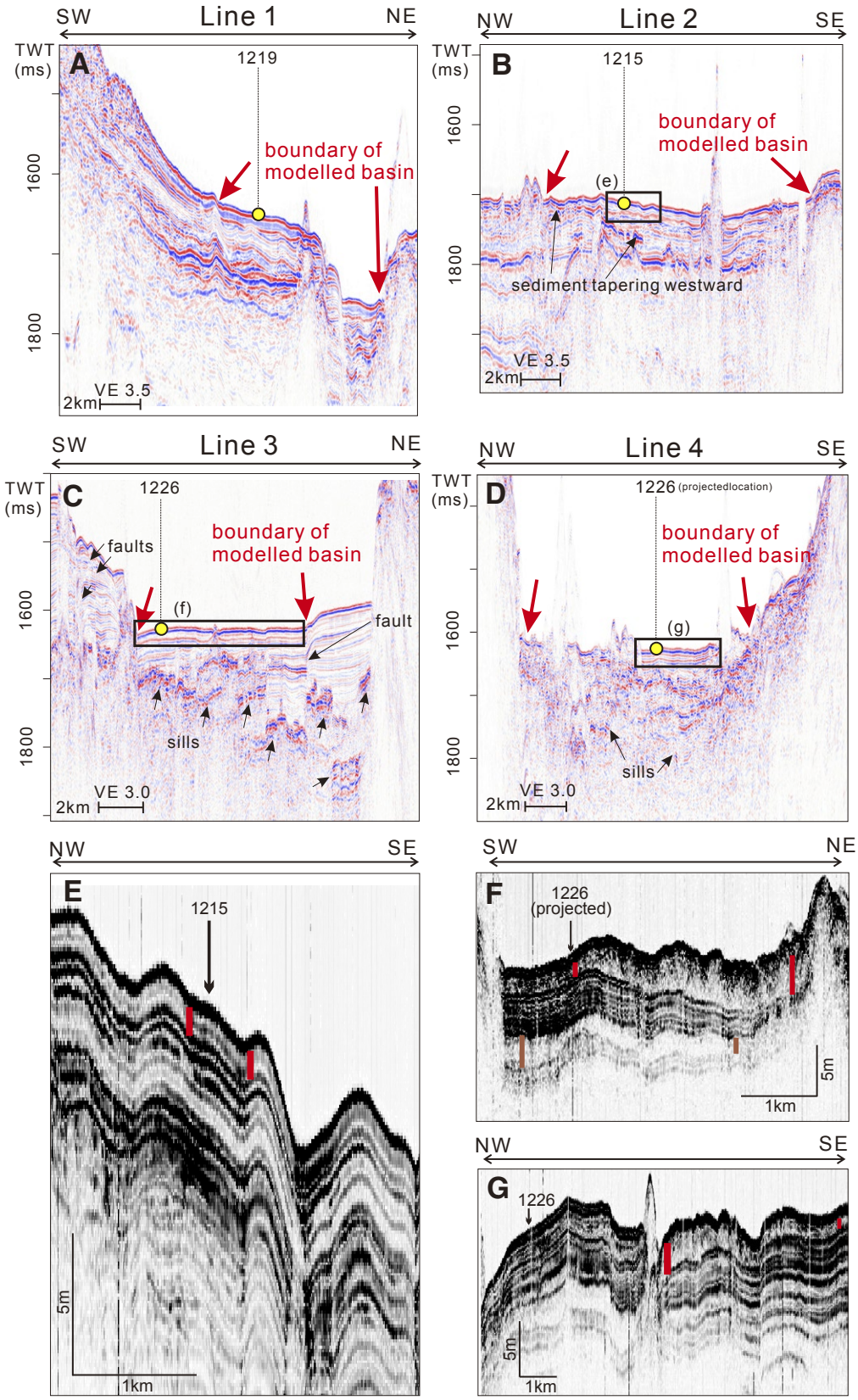

Figure 8. Seismic-reflection data over core sites. (A–D) Multichannel air-gun seismic-reflection images collected along the lines shown in Figure 1. Basin boundaries assigned based on the multibeam data are marked by bold red arrows. (E–G) Parasound sediment profiler records corresponding with the rectangles in (B–D). Vertical red and brown bars illustrate some varied separations of reflections along these lines. TWT—two-way travel time; VE—vertical exaggeration.

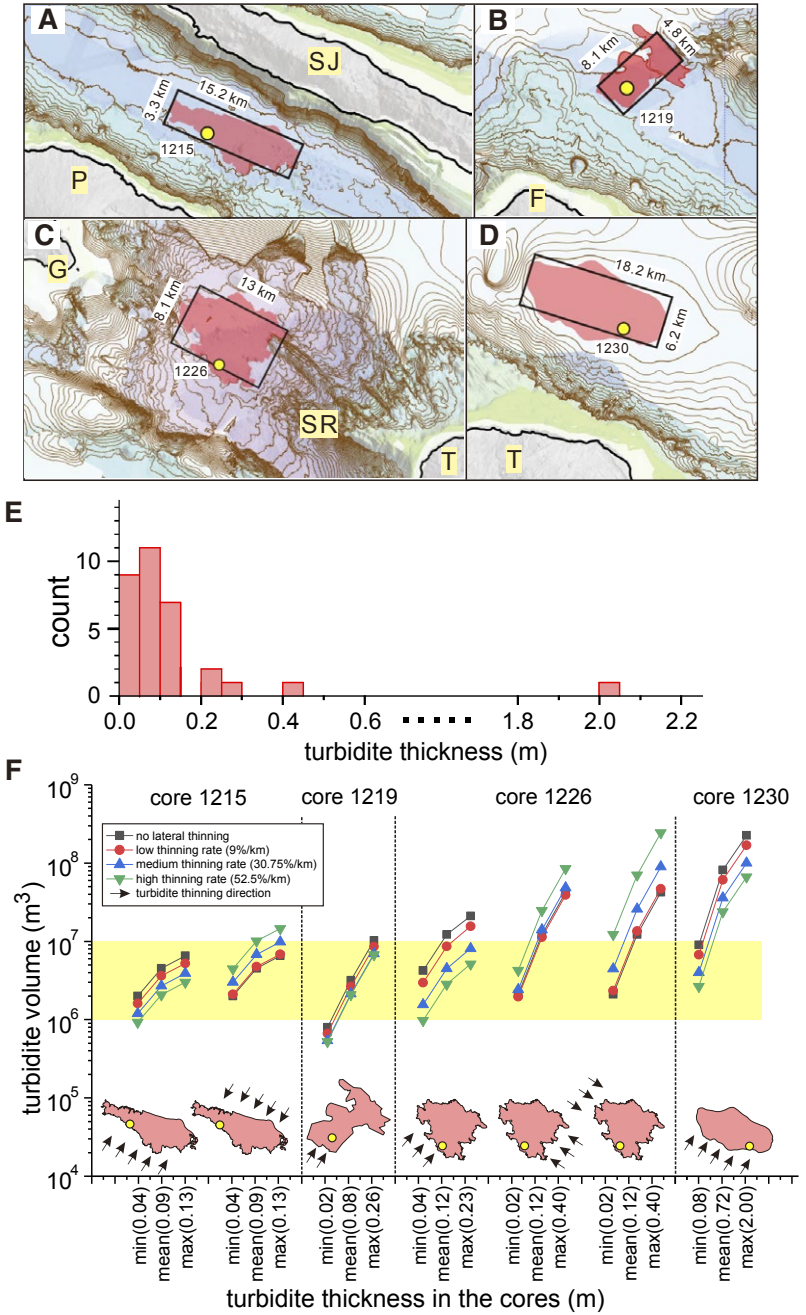

Figure 9. Turbidite volume modeling results. (A–D) Bathymetry (contoured every 50 m) with interpreted turbidite basins (pink) superimposed with rectangles of equal area (black outlines). Yellow circles locate sediment cores. Abbreviations as in Figure 1. (E) Thickness distribution of volcaniclastic beds of the four gravity cores combined. (F) Turbidite volumes for each core modeled with various thinning rates, sediment input directions, and range of turbidite thicknesses found in the cores. Yellow block encompasses the dominant range of modeled turbidite volumes.

volumes and ignimbrite volumes); therefore, this is not such a concern. The moderate thinning rate (i.e., 30.75%/km; blue curves in Fig. 9F) therefore should provide the best volume estimates for large turbidites. This rate is also supported by another transparent section below (brown bars), which tapers eastward from 3.18 to 1.51 m thickness over a distance of 3.05 km, representing a thinning rate of 27%. Similar thinning can be observed in Figure 8G.

For the modeling (Fig. 9F), sediment input directions for PVTs in cores 1219 and 1230 were both chosen from the south sides of the basins, based on the proximity of Faial and Terceira Islands. Core 1215 was interpreted as having received PVTs and SVTs mainly from Pico and São Jorge Islands. Although some sediment flows originating from large events (pyroclastic density currents or landslides) may have traveled longitudinally along the basin floor, the mostly uniform interval of reflections in the Parasound data collected parallel to Pico and São Jorge (Fig. 8E) suggests that such events have been infrequent. We considered three potential sources of turbidity currents for core 1226: Graciosa Island, Serreta Ridge, and escarpment southwest of site 1226. Modest carbonate contents (10%–20%; Chang et al., 2021) in the SVTs of core 1226 could imply that they originated from Graciosa Island, as carbonates from shelf biogenic production would be expected to be common if turbidites were sourced from the island slopes. However, commonly observed young Holocene pyroclastic particles suggest that most SVTs probably are not sourced from Graciosa Island (where explosive eruptions have stopped; Larrea et al., 2014). In practice, the escarpment southwest of site

TABLE 2. MODELED AGES AND VOLUMES OF VOLCANICLASTIC TURBIDITES

Volcaniclastic deposit number	Core ID	Bed thickness (cm)	Bed type	*Estimated calendar age (cal yr B.P.)	Best turbidite volume estimates (10^6 m^3)
1	1215	4	SVT	3878	2.10
2	1215	4	SVT	5262	2.10
3	1215	4	PF	6818	NA
4	1215	13	SVT	11,542	6.85
5	1215	13	SVT	13,406	6.85
6	1215	11	PVT	≥13,406	5.79
7	1215	7	PF	≥13,406	NA
8	1219	10	PVT	811	2.64
9 (C11 eruption)	1219	6	PVT	974	1.58
10	1219	9	PVT	1703	2.37
11	1219	9	PVT	1703	2.37
12	1219	4	SVT	1703	1.06
13	1219	7	SVT	1703	1.85
14	1219	2	PF	11,695	NA
15	1219	7	PVT	17,316	1.85
16	1219	26	PVT	19,559	6.87
17	1219	3	SVT	25,041	0.79
18	1219	2	SVT	40,037	0.53
19	1219	14	PF	45,851	NA
20	1219	5	SVT	88,388	1.31
21	1226	23	PF	627	NA
22	1226	9	SVT	627	3.37
23	1226	5	PVT	627	6.03
24	1226	23	SVT	959	8.88
25	1226	14	PVT	959	16.33
26	1226	40	PVT	959	48.25
27	1226	7	PVT	959	8.17
28	1226	13	PVT	959	15.17
29	1226	4	PVT	2849	4.82
30	1226	2	PVT	3059	2.41
31	1226	2	PVT	3269	2.41
32	1226	4	SVT	3203	1.55
33	1226	17	PF	3203	NA
34	1226	10	PVT	3203	12.05
35	1230	23	SVT	8345	11.47
36	1230	8	PVT	11,261	3.99
37	1230	9	PVT	22,638	4.49
38	1230	1	PF	24,496	NA
39	1230	2	PF	26,146	NA
40	1230	3	PF	26,972	NA
41 (Lajes eruption)	1230	200	PVT	27,179	99.72

Notes: PF—pyroclastic fallout; PVT—primary volcaniclastic turbidite; SVT—secondary volcaniclastic turbidite; NA—none applicable.
*Estimated assuming linear deposition through hemipelagic intervals between known dates.

1226 is suggested to be the most likely source of SVTs as it is an active tectonic feature (the southerly fault escarpment of the Terceira Rift). Volume calculations with the southerly source were therefore only applied to SVTs for core 1226. The common Holocene pyroclastic particles also in the PVTs of core 1226 are suggested to have been dominantly originated from the Serreta Ridge, which has been active in recent times (Gaspar et al., 2003; Madureira et al., 2017; Casas et al., 2018; Romer et al., 2019). Hence, we chose an origin from the SE for the PVTs in this core.

The modeled volumes are 10^5–10^9 m^3 but mostly 10^6–10^7 m^3 (yellow bar in Fig. 9F). The best estimated volumes of individual turbidites were calculated (Table 2) with the preferred 30.75%/km distal thinning rate and the most likely sediment entry direction in each case. Because PVTs and SVTs in core 1215 were potentially emplaced from either Pico or São Jorge Islands, the best estimated volume for each turbidite was an average of the volumes estimated with those two alternative origins. Volumes in Figure 9F vary by up to two orders of magnitude due to bed thickness variations and by up to one order of magnitude because of varied thinning rates.

5. DISCUSSION

5.1 Implications of the Turbidite Volume Estimates

5.1.1 Comparing SVT Volumes with Upper Slope Landslide Volumes

The estimated volumes of SVTs range from 10^5 to 10^8 m^3 (Fig. 10), whereas the landslide valleys in the upper submarine slopes adjacent to the core sites have volumes of 10^2 to 10^8 m^3 (dark-orange bars in Fig. 10). The estimated SVT volumes therefore overlap only the volumes of the larger landslide valleys, suggesting that only the larger deposits of landslide origin have been preserved in the cores. Sediment gravity flows initiated by smaller landslides probably deposited on the slopes before reaching core sites produced thin

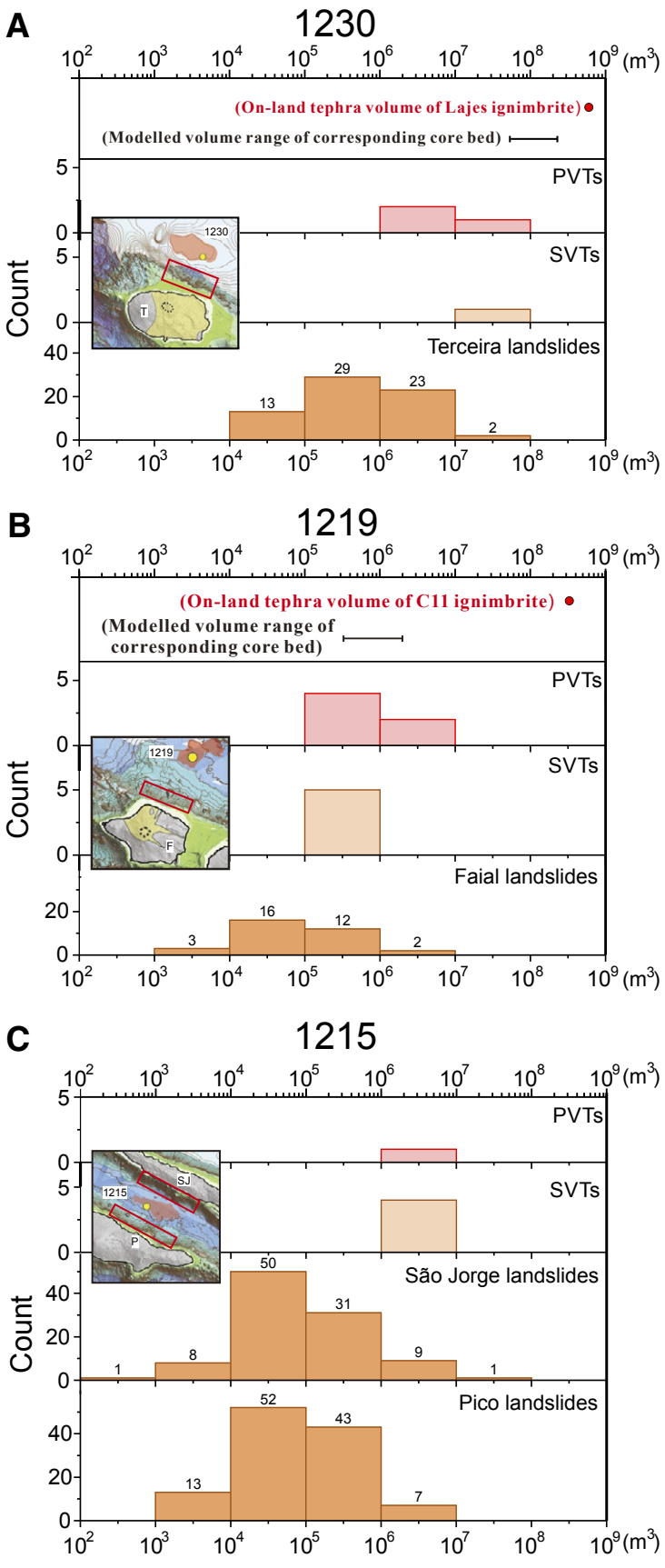

Figure 10. Volumes of basin-floor turbidites predicted with 30.75%/km (intermediate) thinning rates (pink and light-orange histograms) for cores 1230, 1219, and 1215 compared with volumes of landslide valleys in their adjacent upper submarine slopes (dark-orange histograms) derived from Chang et al. (2022b). Also shown are (red dot in A) estimated on-land tephra volume of the Lajes erupted materials from Pimentel et al. (2021) and (red dot in B) estimated tephra volume (on land and offshore) of the C11 erupted materials from Pimentel et al. (2015). Slope regions selected for landslide valley volumes are located by red rectangles on maps. SVTs and PVTs represent secondary and primary volcaniclastic turbidites. The volumes of Pimentel et al. (2015, 2021) and our modeled volumes of PVTs and SVTs are tephra volumes, hence not dense rock equivalents (corrected for pore volumes). Abbreviations as in Figure 1.

beds in the basin floors that cannot be identified by eye or were later obscured by bioturbation.

The turbidites from the larger landslides in the Azores submarine slopes (i.e., >10^6 m^3) should therefore be preserved within these proximal basins. These deposits are smaller than the so-called "giant landslides" reported in the literature (e.g., >10^{11}–10^{12} m^3; Hunt et al., 2013). Our comparison suggests a more comprehensive landsliding history, encompassing smaller volumes, can be preserved in the depositional areas adjacent to the islands, as also found in the continental margins (e.g., Jobe et al., 2018, and references therein). Landsliding inventories are also potentially available for other volcanoes with similar proximal basins.

5.1.2 Comparing PVT Volumes for the C11 and Lajes Eruptions

The PVT volumes allow an assessment of the proportion of pyroclastic sediments transported into the sea and allow us to update estimates of total erupted volumes from the C11 and Lajes events. The best estimated volume of the PVT that is associated with the Lajes eruption in core 1230 (Fig. 10A) is 10^8 m^3 (5×10^7 to 2×10^8 m^3, a range due to the different thinning rates). The volume is of similar order of magnitude but slightly less than the 5.9×10^8 m^3 of the on-land bulk volume of Lajes ignimbrite estimated by Pimentel et al. (2021). A significant portion (8%–33%) of the erupted products was therefore discharged into the ocean and reached the basin floor. We can thus adjust the total volume of erupted pyroclastic products of the Lajes eruption to at least 6.9×10^8 m^3.

The estimated volume of the PVT corresponding to the C11 eruption (Fig. 10B) is 1.58×10^6 m^3. This is at least two orders of magnitude smaller than the volume (>2.2×10^8 m^3) of the ignimbrite on land estimated by Pimentel et al. (2015). Two factors may explain this volume difference. First, the two initial eruptive phases led to deposition mostly toward the north and northwest of the caldera on Faial (inset map to Fig. 10B). The basin-floor sediments may have mainly been emplaced during the last phase of pyroclastic density currents, which Pimentel et al. (2015) showed had a more northeasterly component. Second, the seismic section in Figure 8A suggests that sediments were likely also deposited widely on the upper island slopes rather than solely in the basin floor, which leads to an underestimation of the actual volume.

Because ignimbrite-forming eruptions have occurred repeatedly on Terceira, the island is likely to host similar eruptions in the future (Pimentel et al., 2021). Precisely estimating the areas to be affected by erupted products is difficult for small volcanic islands because the portions of products transported offshore are usually unclear (Walker, 1981). Our tephra correlations imply that the C11 and Lajes deposits extend offshore at least 20–30 km, a distance three to five times farther than the outcrops on land had suggested. The turbidite volume modeling also indicates that a significant portion of the Lajes ignimbrite discharged into the sea. We suggest that further sediment cores from the slopes and around the basins would be desirable to constrain better the distal thickness variations and total volumes. This should include the basin south of Terceira, given that the Lajes ignimbrite also extended southwards.

5.1.3 Comparing Sediment Fluxes in Source Areas with Depositional Fluxes in Basins

The radiocarbon-dated sediments allow depositional fluxes in the basins to be compared with fluxes of sediment released by erosion on the islands, eruptive activity, and biogenic production on their shelves during the Holocene. Quartau et al. (2012) showed that the present sediments on the shelf of Faial Island are all Holocene in age because there is no evidence of older stratigraphy in boomer seismic records from there. They estimated fluxes for the past 6.5 k.y. from onshore and shelf sources for ~1/4 of the island (their sectors F and G in their table 3). We divided those fluxes by a factor of two to allow for the smaller length of the north coastline of Faial adjacent to the basin containing core site 1219. The estimated total sediment flux to the basin of 45.2×10^6 m^3/k.y. includes subaerial sources (pyroclastics from recent eruptions, cliff erosion, and riverine erosion) of 44×10^6 m^3/k.y. and submarine sources (bioclasts) of 1.2×10^6 m^3/k.y.

We can also assess how much particle accumulation has occurred in the hemipelagic deposits, some of which likely comprise fine particles also originating from the island (e.g., remobilized volcanic ash). The flux in the basin of core 1219 was estimated to have been 3×10^6 m^3/k.y. by assuming that a constant average hemipelagic sedimentation rate occurred uniformly over the basin polygon during the 0–8 k.y. period. This is only 6.7% of the island-generated flux.

We can also compare the island fluxes with those of the SVTs, which contain some reworked material possibly originating from the island shelf and coasts. The mean SVT flux was 1.1×10^6 m^3/k.y. obtained by dividing the total turbidite volume in the basin by the SVT emplacement interval in core 1219 (0–8 k.y.). This depositional flux is only ~2.4% of the island-generated flux. There is therefore a large difference (90.9%) between the flux supplied from the island and the combined hemipelagic and SVT fluxes in the basin. This discrepancy is a minimum, as a further component of the sediment originated from the tests of pelagic organisms originating from the overlying water column.

The flux discrepancy also supports our earlier inference based on the SVT volumes that smaller landslides produce sediment gravity flows that deposit on the slopes. Thick sequences of reflections dipping parallel to seabed are commonly observed within the flanks of oceanic islands (e.g., the Hawaiian Islands [Leslie et al., 2002]; the Marquesas Islands [Wolfe et al., 1994]; and the Canary Islands [Watts et al., 1997; León et al., 2017]). These are likely at least partly due to clastic deposits from sediment gravity flows that have not fully runout. Some shallow examples of such reflections are shown in Figure 8A.

5.2 Has Sediment Deposition History Been Affected by Climatic Changes?

Both hemipelagic sedimentation rates and frequencies of submarine landsliding were generally higher during the time of sea-level highstand

(0–8 k.y.) than during the sea-level transgression or regression (Fig. 7A), suggesting a potential climatic influence.

5.2.1 Hemipelagic Sedimentation Rates

The increased hemipelagic sedimentation rates during the Holocene sea-level highstand period in this study differ from the predictions of classical siliciclastic sequence stratigraphy models (Posamentier and Vail, 1988; Posamentier et al., 1988), which usually suggest decreasing highstand rates in deep-water slopes. Accordingly, shelves are exposed, and most slopes are connected by rivers or ice streams (e.g., Covault and Graham, 2010) during sea-level lowstands on continental margins, enhancing sediment transport through cross-shelf valleys to the slope and basin floors. However, riverine supply of sediment in the Azores islands is minor compared to supply by shelf biogenic production, coastal erosion, and volcanism (e.g., Quartau et al., 2012; Ramalho et al., 2013) due to the lack of permanent streams and weak orographic precipitation (Forjaz et al., 2004; Instituto Nacional de Meteorologia, 2012). Sediment inputs around insular volcanic islands differ due to several factors. For instance, the insular shelves of volcanic islands submerged during sea-level highstands allow increased biogenic production that would not occur if the shelves were exposed above sea level (e.g., Ramalho et al., 2013). High sea level also allows waves to attack and erode the tall sea cliffs (e.g., Zhao et al., 2020), which Quartau et al. (2012) suggested to be the primary source of sediments to the shelf of Faial. In contrast, sea cliffs should be more protected from wave attack when sea level was even only a few tens of meters lower than at present. The high emplacement frequencies of PVTs in cores 1219 and 1226 (Fig. 7C) during the Holocene suggest that increased pyroclastic activity could also be a reason for the increased hemipelagic sedimentation rates due to the additional supply of easily erodible volcaniclastic products. The high hemipelagic sedimentation rate in core 1215 is further probably due to dual sediment inputs from both Fail and Pico Islands.

5.2.2 Frequencies of Secondary Volcaniclastic Turbidite Emplacements

Many of the upper-slope landslides in the Azores have been suggested to have been triggered by ground shaking during earthquakes (Chang et al., 2022b). As earthquakes typically occur randomly over time, they do not clearly explain the increase in SVT emplacements into the sea-level highstand period. However, increased earthquake activity may be genetically connected to periods of increased magmatic activity. Seismogenic faults are common among the islands (Madeira et al., 2015), and many faults in sea areas between them are seismogenic also based on the pattern of seismicity (Casalbore et al., 2015; Mitchell et al., 2018). GPS measurements further suggest widespread displacements from distributed tectonic deformation and volcano deformation (D'Araújo et al., 2022).

Sidescan sonar and grain-size data suggest that sediment released by coastal erosion is transported toward the outer shelves and upper slopes of the islands (Chang et al., 2022a). As such sediment fluxes are likely greater during highstand conditions (Quartau et al., 2012), more rapid deposition onto the upper slopes can be expected. The amount of time for such deposits to over-steepen and/or become thick enough to generate large sediment gravity flows when failed will also be shortened. The increased frequency of SVT seems therefore more likely associated with higher sediment fluxes toward the present day.

The enhanced frequencies of highstand SVT emplacement and hemipelagic rates prompt us to question whether the changes in the source fluxes we propose ultimately affected the volumes of SVTs in the basins; i.e., did a larger flux of sediment from the shelves lead to larger landslides and hence larger SVTs? Chang et al. (2022b) found that landslide scar volumes differ between the different islands, with larger volumes of scars in the slopes of São Jorge and Terceira Islands compared with Pico and Faial Islands. The shelves of São Jorge and Terceira Islands are wider than those of Pico and Faial Islands; hence, they have accumulated greater volumes of sediment from biogenic production during the Holocene highstand period Consequently, greater sediment spillover of sediment to the slopes might be expected, leading to thicker accumulations of unstable sediment before failure between major earthquakes. Figure 11, however, shows no significant systematic variation in best estimated SVT volumes with age. Investigating this issue will require additional analyses of cores around the islands to compensate for the data variability.

5.2.3 Frequencies of Primary Volcaniclastic Turbidite Emplacements

Primary volcaniclastic turbidite (PVT) emplacements became more frequent overall in the sea-level highstand period (Fig. 7A), but changes in PVT frequencies vary between cores (light-tone colors in Fig. 7C) reflecting different explosive sources. For instance, PVT frequency was similar in both transgression and highstand periods for core 1215, whereas it decreased for core 1230. In contrast, PVT frequencies for core 1219 increased into the highstand period (given the age constraints, this inference holds up even if bed 16 in the core has been mis-assigned; Fig. 2). Frequencies for core 1226 were also high in the highstand period, although we have no data on previous times.

Since each core had different predominant volcanic sources, there is no evidence that those sources reacted in any coordinated way to sea level and/or climate changes. Thus, we find no evidence for increased volcanic activity due to unloading during the low sea-level stand (Hasenclever et al., 2017), and we also find no evidence for the suppression of eruptions by stresses induced by sea-level rise as proposed for Santorini (Satow et al., 2021). The Azores islands also have elevations that are too low for glaciers to have been widespread at this latitude during the last ice age. The equilibrium line altitudes of glaciers in Spain at similar latitudes (Palacios et al., 2017; Serrano et al., 2017) are higher than the highest elevation in the Azores (Mount Pico, 2351 m).

There is also no resolvable systematic change in PVT volumes between transgression dates and highstand periods overall (Fig. 11B). PVT volumes

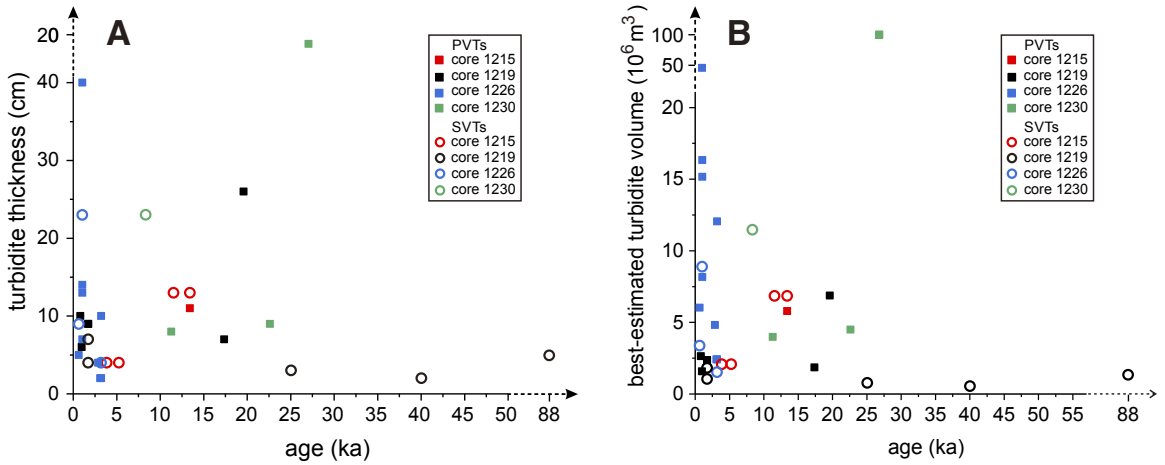

Figure 11. Temporal variations in (A) turbidite thicknesses and (B) best estimated turbidite volumes. PVTs and SVTs are primary volcaniclastic turbidites and secondary volcaniclastic turbidites, respectively.

for cores 1219 and 1226 are similar to the SVT volumes at those sites, with no obvious change with time. PVT volumes in core 1219 are small compared to PVT volumes in other cores. In contrast, PVT volumes in core 1226 vary more than in other cores, possibly a result of some or all turbidites being sourced from the Serreta Ridge (e.g., Casalbore et al., 2015; Casas et al., 2018). The lack of a common variation in eruption frequency and erupted volumes with time among the cores suggests that eruptions were not modulated by direct or indirect climatic influence. Rather, temporal variations are more likely a result of variations in magma supply or tectonic processes affecting eruptions (e.g., Kappel and Ryan, 1986). Further work on the chronology of eruptions in the Azores would help evaluate whether a subtler change in eruption frequency nevertheless occurred.

6. CONCLUSIONS

Four chronostratigraphies have been developed based on 12 calibrated radiocarbon dates from hemipelagic beds in these four sediment cores and from two pyroclastic turbidites correlated with ignimbrites formed on Faial Island (C11 at ca 1.0 ka) and Terceira Island (Lajes at ca. 25 ka). Age-depth models for the hemipelagic components were reconstructed to date the emplacements of turbidites and tephra in each core to a maximum age of ca. 50 ka. Return periods of eruptions and landslides large enough to generate turbidites within the cores were found to be mostly >1 k.y. for both turbidite types. Hemipelagic sedimentation rates and submarine landslide frequencies were higher in the past 8 k.y. than in the previous few tens of thousands of years. The increased hemipelagic sedimentation rate could be explained by sea-level rise, which enhances erosion of subaerial sea cliffs and biogenic production on shelves. More frequent emplacements of pyroclastic turbidites were found in some cores for the past 8 k.y.; if this occurred more widely, eruptions also supplied more friable volcaniclastic products to submarine and subaerial areas. The greater submarine landslide frequency of the past 8 k.y. is probably associated with the greater sediment supply, leading to more rapid build-up of unstable sediment on the submarine slopes of the islands. The higher emplacement frequency of primary volcaniclastic beds in some cores and lack of increase in others during the past 8 k.y. contradicts models that have been proposed in which higher sea level increases the load on magma chamber roofs, leading to lower eruption frequencies. We suggest this different eruption timing may in part be due to temporal variations in magma supply, which can occur in volcanic rifts.

Turbidite volumes have been estimated allowing for varied thinning rates across basin floors and different input directions of sediment flows. The estimated volumes are 10^5–10^9 m^3 (mostly 10^6–10^7 m^3). The volcaniclastic turbidites of landslide origin are comparable in volume with only the largest of their adjacent upper-slope submarine landslide valleys; therefore, most landslides lead to mass flows that deposit on the slopes and do not reach the basins. This inference is also supported by a major difference between sediment export flux of Faial and depositional fluxes of SVTs and hemipelagic sediments in core 1219. We therefore suggest that the dipping seismic reflections found in the flanks of many volcanic ocean islands are mostly due to clastic material from sedimentary flows that did not fully runout to the adjacent basin floors and instead deposited on the slopes.

For two well-dated eruptions, the total volumes of their products and proportions exported offshore

were revised. For the Lajes eruption, 8%–33% of its pyroclastic products were emplaced in the basin north of Terceira; hence the total erupted volume was at least 6.5–8.2 × 10^8 m^3 larger than previously suggested. In contrast, the volume of the turbidite associated with the C11 eruption is two orders of magnitude smaller than the corresponding ignimbrite on land, suggesting that deposits in the basin originated only from one of the eruptive phases or that deposits exported to the sea largely remained on the slopes without reaching the core site.

ACKNOWLEDGMENTS

We thank the scientific party and crew of RV *Meteor* during cruise M141/1 for their work in collecting the gravity cores. This cruise was funded by the DFG (German Research Foundation) and GEOMAR. We also acknowledge the project "Features of Azores and Italian Volcanic Islands (FAIVI)," supported by the European Communities 7th Framework Programme under EUROFLEETS grant agreement no. 228344, which allowed the acquisition of multibeam bathymetry around Terceira Island. John Moore, Jon Yarwood, and Tom Bishop of Manchester Geography Laboratories were very helpful in providing laboratory space and access to a high-power optical microscope for sample preparation. Bor-Jiun Jong, Shunwen Yu, Pei-Chen Kuo, and Chia-Hsin Tsai are thanked for sharing their experience on sample preparation for radiocarbon analysis. Thanks also to Chih-Kai Chuang for sharing his knowledge and experience of identifying foraminiferal species and to Dr. Philippa Ascough for assisting in the Natural Environmental Research Council (NERC) radiocarbon grant application and project management. We especially thank the staff in the environmental Radiocarbon Laboratory at Scottish Universities of Environmental Research Centre for carrying out the radiocarbon analyses. We thank also Science Editor Andrea Hampel and reviewers Adriano Pimentel and Fabiano Gamberi for providing thoughtful comments on the submitted article, which significantly improved it.

The government of Taiwan funded this Ph.D. research with a scholarship. Radiocarbon dating was funded by the Natural Environmental Research Council (NERC) support for Natural Environment Isotope Facility (NEIF grant 2330.0920). The British Geophysical Association Gray-Milne funded attendance at the European Geoscience Union General Assembly 2022, where some of these ideas were discussed. Travel to Germany was funded by an International Exchanges grant from the Royal Society (IES\R3\170081). Further support was provided by NERC grant NE/T014814/1.

The 2003 multibeam data are available at 100 m grid resolution from the Marine Geoscience Data Portal (http://www.marine-geo.org/index.php). The multibeam data for Terceira are not publicly available due to the sensitive nature of the area and environmental sustainability concerns but can be made available to researchers with appropriate credentials. Background bathymetric data are from the Global Multi-Resolution Topography synthesis (Ryan et al., 2009) obtained via the GeoMapApp (www.geomapapp.org).

REFERENCES CITED

Allin, J.R., Hunt, J.E., Talling, P.J., Clare, M.A., Pope, E., and Masson, D.G., 2016, Different frequencies and triggers of canyon filling and flushing events in Nazaré Canyon, offshore Portugal: Marine Geology, v. 371, p. 89–105, https://doi.org/10.1016/j.margeo.2015.11.005.

Ascough, P., Cook, G., and Dugmore, A., 2005, Methodological approaches to determining the marine radiocarbon reservoir effect: Progress in Physical Geography, v. 29, no. 4, p. 532–547, https://doi.org/10.1191/0309133305pp461ra.

Ausín, B., Haghipour, N., Wacker, L., Voelker, A.H.L., Hodell, D., Magill, C., Looser, N., Bernasconi, S.M., and Eglinton, T.I., 2019, Radiocarbon age offsets between two surface dwelling planktonic foraminifera species during abrupt climate events in the SW Iberian margin: Paleoceanography and Paleoclimatology, v. 34, no. 1, p. 63–78, https://doi.org/10.1029/2018PA003490.

Bergh, S.G., and Gudmunder, E.S., 1991, Pleistocene mass-flow deposits of basaltic hyaloclastite on a shallow submarine shelf, South Iceland: Bulletin of Volcanology, v. 53, p. 597–611, https://doi.org/10.1007/BF00493688.

Blaauw, M., 2010, Methods and code for 'classical' age-modelling of radiocarbon sequences: Quaternary Geochronology, v. 5, no. 5, p. 512–518, https://doi.org/10.1016/j.quageo.2010.01.002.

Bonath, E., 1990, Not so hot "hot spots" in the oceanic mantle: Science, v. 250, p. 107–111, https://doi.org/10.1126/science.250.4977.107.

Brock, F., Higham, T., Ditchfield, P., and Ramsey, C.B., 2010, Current pretreatment methods for AMS radiocarbon dating at the Oxford Radiocarbon Accelerator Unit (Orau): Radiocarbon, v. 52, no. 1, p. 103–112, https://doi.org/10.1017/S0033822200045069.

Calvert, A.T., Moore, R.B., McGeehin, J.P., and Rodrigues da Silva, A.M., 2006, Volcanic history and $^{40}Ar/^{39}Ar$ and ^{14}C geochronology of Terceira Island, Azores, Portugal: Journal of Volcanology and Geothermal Research, v. 156, no. 1–2, p. 103–115, https://doi.org/10.1016/j.jvolgeores.2006.03.016.

Cappello, A., Zanon, V., Del Negro, C., Ferreira, T.J.L., and Queiroz, M.G.P.S., 2015, Exploring lava-flow hazards at Pico Island, Azores Archipelago (Portugal): Terra Nova, v. 27, no. 2, p. 156–161, https://doi.org/10.1111/ter.12143.

Carlson, J., and Grotzinger, J.P., 2001, Submarine fan environment inferred from turbidite thickness distributions: Sedimentology, v. 48, no. 6, p. 1331–1351, https://doi.org/10.1046/j.1365-3091.2001.00426.x.

Casalbore, D., Romagnoli, C., Pimentel, A., Quartau, R., Casas, D., Ercilla, G., Hipólito, A., Sposato, A., and Chiocci, F.L., 2015, Volcanic, tectonic and mass-wasting processes offshore Terceira Island (Azores) revealed by high-resolution seafloor mapping: Bulletin of Volcanology, v. 77, p. 24, https://doi.org/10.1007/s00445-015-0905-3.

Casas, D., Pimentel, A., Pacheco, J., Martorelli, E., Sposato, A., Ercilla, G., Alonso, B., and Chiocci, F., 2018, Serreta 1998–2001 submarine volcanic eruption, offshore Terceira (Azores): Characterization of the vent and inferences about the eruptive dynamics: Journal of Volcanology and Geothermal Research, v. 356, p. 127–140, https://doi.org/10.1016/j.jvolgeores.2018.02.017.

Chang, Y.-C., Mitchell, N., Quartau, R., and Hansteen, T., 2021, Landslides in the upper submarine slopes of volcanic islands: The central Azores: Geochemistry, Geophysics, Geosystems, v. 22, no. 10, https://doi.org/10.1029/2021GC009833.

Chang, Y.-C., Mitchell, N., Quartau, R., Hübscher, C., Rusu, L., and Tempera, F., 2022a, Asymmetric abundances of submarine sediment waves around the Azores volcanic islands: Marine Geology, v. 449, https://doi.org/10.1016/j.margeo.2022.106837.

Chang, Y.-C., Mitchell, N.C., Hansteen, T.H., Schindlbeck-Belo, J.C., and Freundt, A., 2022b, Volcaniclastic deposits and sedimentation processes around volcanic ocean islands: The central Azores, *in* Di Capua, A., et al., eds., Volcanic Processes in the Sedimentary Record: When Volcanoes Meet the Environment: Geological Society of London, Special Publication 520, https://doi.org/10.1144/SP520-2021-62.

Chiocci, F.L., Romagnoli, C., Casalbore, D., Sposato, A., Martorelli, E., Alonso, B., Casas, D., Conte, A.M., Bella, L.D., Ercilla, G., Estrada, F., Falese, F., Farran, M., Forleo, V., Frezza, V., Hipolito, A., Lebani, A., Maisto, F., Pacheco, J., Pimentel, A., Quartau, R., Roque, C., Sampaio, I., Santoro, P.C., and Tempera, F., 2013, Bathy-morphological setting of Terceira Island (Azores) after the FAIVI cruise: Journal of Maps, v. 9, p. 590–595, https://doi.org/10.1080/17445647.2013.831381.

Clare, M.A., Talling, P.J., and Hunt, J.E., 2015, Implications of reduced turbidity current and landslide activity for the Initial Eocene Thermal Maximum—Evidence from two distal, deep-water sites: Earth and Planetary Science Letters, v. 420, p. 102–115, https://doi.org/10.1016/j.epsl.2015.03.022.

Cole, P., Guest, J., Duncan, A., and Pacheco, J.-M., 2001, Capelinhos 1957–1958, Faial, Azores: Deposits formed by an emergent surtseyan eruption: Bulletin of Volcanology, v. 63, no. 2, p. 204–220, https://doi.org/10.1007/s004450100136.

Costa, A.C.G., Marques, F.O., Hildenbrand, A., Sibrant, A.L.R., and Catita, C.M.S., 2014, Large-scale flank collapses in a steep volcanic ridge: Pico-Faial Ridge, Azores Triple Junction: Journal of Volcanology and Geothermal Research, v. 272, p. 111–125, https://doi.org/10.1016/j.jvolgeores.2014.01.002.

Costa, A.C.G., Hildenbrand, A., Marques, F.O., Sibrant, A.L.R., and Santos de Campos, A., 2015, Catastrophic flank collapses and slumping in Pico Island during the last 130 kyr (Pico-Faial ridge, Azores Triple Junction): Journal of Volcanology and Geothermal Research, v. 302, p. 33–46, https://doi.org/10.1016/j.jvolgeores.2015.06.008.

Coussens, M., Wall-Palmer, D., Talling, P.J., Watt, S.F.L., Cassidy, M., Jutzeler, M., Clare, M.A., Hunt, J.E., Manga, M., Gernon, T.M., Palmer, M.R., Hatter, S.J., Boudon, G., Endo, D., Fujinawa, A., Hatfield, R., Hornbach, M.J., Ishizuka, O., Kataoka, K., Le Friant, A., Maeno, F., McCanta, M., and Stinton, A.J., 2016, The relationship between eruptive activity, flank collapse, and sea level at volcanic islands: A long-term (>1 Ma) record offshore Montserrat, Lesser Antilles: Geochemistry, Geophysics, Geosystems, v. 17, no. 7, p. 2591–2611, https://doi.org/10.1002/2015GC006053.

Covault, J.A., and Graham, S.A., 2010, Submarine fans at all sea-level stands: Tectono-morphologic and climatic controls on terrigenous sediment delivery to the deep sea: Geology, v. 38, no. 10, p. 939–942, https://doi.org/10.1130/G31081.1.

D'Araújo, J., Sigmundsson, F., Ferreira, T., Okada, J., Lorenzo, M., and Silva, R., 2022, Plate boundary deformation and volcano unrest at the Azores triple junction determined from continuous GPS measurements, 2002–2017: Journal

of Geophysical Research Solid Earth, v. 127, 14 p., https://doi.org/10.1029/2021JB023007.

Féraud, G., Kaneoka, I., and Allegre, C.J., 1980, K/Ar ages and stress pattern in the Azores: Dynamic implications: Earth and Planetary Science Letters, v. 46, p. 275–286, https://doi.org/10.1016/0012-821X(80)90013-8.

Fierstein, J., and Nathenson, M., 1992, Another look at the calculation of fallout tephra volumes: Bulletin of Volcanology, v. 54, no. 2, p. 156–167, https://doi.org/10.1007/BF00278005.

Forjaz, V.H., Tavares, J.M., Azevedo, E.M.V.B., Nunes, J.C., Santos, R.S., Barreiros, J.P., Gallagher, L., Barcelos, P.J.M., Silva, P.H., Cardigos, F., França, Z.T.M., Dentinho, T., Costa, M.P., Magalhães, L., Rodrigues, M.C., Gonçalves, J.F., Silva, V., and Serpa, V., 2004, Atlas Básico dos Açores (2nd edition): Observatório Vulcanológico e Geotérmico dos Açores, 112 p.

Gaspar, J.L., Queiroz, G., Pacheco, J.A., Ferreira, T., Wallenstein, N., Almeida, M.H., and Coutinho, R., 2003, Basaltic lava balloons produced during the 1998–2001 Serreta Submarine Ridge eruption (Azores), *in* White, J.D.L., Smellie, J.L., and Clague, D.A., eds., Subaqueous Explosive Volcanism: Washington, D.C., American Geophysical Union Geophysical Monograph 140, p. 205–212. https://doi.org/10.1029/140GM13.

Gaspar, J.L., Queiroz, G., Ferreira, T., Medeiros, A.R., Goulart, C., and Medeiros, J., 2015, Earthquakes and volcanic eruptions in the Azores region: Geodynamic implications from major historical events and instrumental seismicity, *in* Gaspar, J.L., Guest, J.E., Duncan, A.M., Barriga, F.J.A.S., and Chester, D.K., eds., Volcanic Geology of São Miguel Island (Azores Archipelago): Geological Society of London, Memoir 44, p. 33–49, https://doi.org/10.1144/M44.4.

Gente, P., Dyment, J., Maia, M., and Goslin, J., 2003, Interaction between the Mid-Atlantic Ridge and the Azores hot spot during the last 85 Myr: Emplacement and rifting of the hot spot-derived plateaus: Geochemistry, Geophysics, Geosystems, v. 4, no. 10, 23 p., https://doi.org/10.1029/2003GC000527.

Gertisser, R., Self, S., Gaspar, J.L., Kelley, S.P., Pimentel, A., Eikenberg, J., Barry, T.L., Pacheco, J.M., Queiroz, G., and Vespa, M., 2010, Ignimbrite stratigraphy and chronology on Terceira Island, Azores, *in* Groppelli, G., and Viereck-Goette, L., eds., Stratigraphy and Geology of Volcanic Areas: Geological Society of America Special Paper 464, p. 133–154. https://doi.org/10.1130/2010.2464(07).

Glazner, A.F., Manley, C.R., Marron, J.S., and Rojstaczer, S., 1999, Fire or ice: Anticorrelation of volcanism and glaciation in California over the past 800,000 years: Geophysical Research Letters, v. 26, no. 12, p. 1759–1762, https://doi.org/10.1029/1999GL900333.

Gràcia, E., Vizcaino, A., Escutia, C., Asioli, A., Rodés, Á., Pallàs, R., Garcia-Orellana, J., Lebreiro, S., and Goldfinger, C., 2010, Holocene earthquake record offshore Portugal (SW Iberia): Testing turbidite paleoseismology in a slow-convergence margin: Quaternary Science Reviews, v. 29, no. 9-10, p. 1156–1172, https://doi.org/10.1016/j.quascirev.2010.01.010.

Gutierrez-Pastor, J., Nelson, C.H., Goldfinger, C., Johnson, J.E., Escutia, C., Eriksson, A., and Morey, A.E., and The Shipboard Scientific Party, 2009, Earthquake control of Holocene turbidite frequency confirmed by hemipelagic sedimentation chronology on the Cascadia and Northern California active continental margins, *in* Kneller, B., Martinsen, O.J., and McCaffrey, B., eds., External Controls on Deep-Water Depositional Systems: SEPM (Society for Sedimentary Geology), v. 92, https://doi.org/10.2110/sepmsp.092.179.

Hajdas, I., 2008, Radiocarbon dating and its applications in Quaternary studies: E&G Quaternary Science Journal, v. 57, no. 1/2, p. 2–24, https://doi.org/10.3285/eg.57.1-2.1.

Hall, K., 1982, Rapid deglaciation as an initiator of volcanic activity: An hypothesis: Earth Surface Processes and Landforms, v. 7, no. 1, p. 45–51, https://doi.org/10.1002/esp.3290070106.

Hansteen, T.H., Freundt, A., and Kutterolf, S., 2017, Short cruise report RV METEOR M141/1: Azores tephras: GEOMAR Helmholtz-Zentrum für Ozeanforschung Kiel, https://www.ldf.uni-hamburg.de/meteor/wochenberichte/wochenberichte-meteor/m141-m145/m141-scr.pdf.

Hasenclever, J., Knorr, G., Rüpke, L.H., Köhler, P., Morgan, J., Garofalo, K., Barker, S., Lohmann, G., and Hall, I.R., 2017, Sea level fall during glaciation stabilized atmospheric CO_2 by enhanced volcanic degassing: Nature Communications, v. 8, https://doi.org/10.1038/ncomms15867.

Heaton, T.J., Köhler, P., Butzin, M., Bard, E., Reimer, R.W., Austin, W.E.N., Bronk Ramsey, C., Grootes, P.M., Hughen, K.A., Kromer, B., Reimer, P.J., Adkins, J., Burke, A., Cook, M.S., Olsen, J., and Skinner, L.C., 2020, Marine20—The marine radiocarbon age calibration curve (0–55,000 cal BP): Radiocarbon, v. 62, no. 4, p. 779–820, https://doi.org/10.1017/RDC.2020.68.

Hildenbrand, A., Weis, D., Madureira, P., and Marques, F.O., 2014, Recent plate re-organization at the Azores Triple Junction: Evidence from combined geochemical and geochronological data on Faial, S. Jorge and Terceira volcanic islands: Lithos, v. 210–211, p. 27–39, https://doi.org/10.1016/j.lithos.2014.09.009.

Hübscher, C., 2013, Tragica—Cruise No. M79/2—August 26–September 21, 2009–Ponta Delgada (Azores/Portugal)–Las Palmas (Canary Islands/Spain): DFG–Senatskommission für Ozeanographie, p. 2195–8475.

Hübscher, C., and Gohl, K., 2014, Reflection/Refraction Seismology, *in* Harff, J., Meschede, M., Petersen, S., and Thiede, J., eds., Encyclopedia of Marine Geosciences: Dordrecht, Netherlands, Springer, p. 1–15, https://doi.org/10.1007/978-94-007-6644-0_128-1.

Hübscher, C., Beier, C., Al-Hseinat, M., Batista, L., Blum, M., Bobsin, M., Bülow, J., Frahm, L., Grob, H., Hildenbrandt, A., Kalvelage, C., Kammann, J., Knevels, K., Levanos, I., Nomikou, P., Reichel, H., Petry, F., Spickermann, D., Stackemann, F., Stratmann, S., Terrinha, P., Vögele, M., Winter, S., Schaaf, T., Schleifer, B., Stelzner, M., Spitzy, S., Weinzierl, C., and Weiß, B., 2016, Azores Plateau—Cruise No. M113/1—December 29, 2014–January 22, 2015–Ponta Delgada (Portugal)–Ponta Delgada (Portugal): DFG–Senatskommission für Ozeanographie, p. 2195–8475.

Hunt, J.E., Wynn, R.B., Talling, P.J., and Masson, D.G., 2013, Multistage collapse of eight western Canary Island landslides in the last 1.5 Ma: Sedimentological and geochemical evidence from subunits in submarine flow deposits: Geochemistry, Geophysics, Geosystems, v. 14, no. 7, p. 2159–2181, https://doi.org/10.1002/ggge.20138.

Instituto Nacional de Meteorologia, 2012, Atlas climatico de los Archipielagos de Canarias, Madeira y Azores temperatura del aire y precipitacion (1971–2000): Lisboa, Instituto de Meteorologia.

Jellinek, A.M., Manga, M., and Saar, M.O., 2004, Did melting glaciers cause volcanic eruptions in eastern California?: Probing the mechanics of dike formation: Journal of Geophysical Research. Solid Earth, v. 109, B09206, https://doi.org/10.1029/2004JB002978.

Jobe, Z.R., Howes, N., Romans, B.W., and Covault, J.A., 2018, Volume and recurrence of submarine-fan-building turbidity currents: The Depositional Record: A Journal of Biological, Physical and Geochemical Sedimentary Processes, v. 4, no. 2, p. 160–176, https://doi.org/10.1002/dep2.42.

Kappel, E.S., and Ryan, W.B.F., 1986, Volcanic episodicity and a non-steady state rift valley along northeast Pacific spreading centers: Evidence from Sea MARC I: Journal of Geophysical Research, v. 91, p. 13,925–13,940, https://doi.org/10.1029/JB091iB14p13925.

Kutterolf, S., Freundt, A., Perez, W., Mörz, T., Schacht, U., Wehrmann, H., and Schmincke, H.U., 2008, Pacific offshore record of plinian arc volcanism in Central America: 1. Along-arc correlations: Geochemistry, Geophysics, Geosystems, v. 9, no. 2, https://doi.org/10.1029/2007GC001631.

Kutterolf, S., Freundt, A., and Burkert, C., 2011, Eruptive history and magmatic evolution of the 1.9 kyr Plinian dacitic Chiltepe Tephra from Apoyeque volcano in west-central Nicaragua: Bulletin of Volcanology, v. 73, no. 7, p. 811–831, https://doi.org/10.1007/s00445-011-0457-0.

Kutterolf, S., Schindlbeck, J.C., Jegen, M., Freundt, A., and Straub, S.M., 2019, Milankovitch frequencies in tephra records at volcanic arcs: The relation of kyr-scale cyclic variations in volcanism to global climate changes: Quaternary Science Reviews, v. 204, p. 1–16, https://doi.org/10.1016/j.quascirev.2018.11.004.

Lal, D., and Peters, B., 1967, Cosmic ray produced radioactivity on the Earth, *in* Sitte, K., ed., Kosmische Strahlung II/Cosmic Rays II: Berlin, Heidelberg, Springer, p. 551–612, https://doi.org/10.1007/978-3-642-46079-1_7.

Larrea, P., Wijbrans, J.R., Galé, C., Ubide, T., Lago, M., França, Z., and Widom, E., 2014, $^{40}Ar/^{39}Ar$ constraints on the temporal evolution of Graciosa Island, Azores (Portugal): Bulletin of Volcanology, v. 76, no. 2, p. 1–15, https://doi.org/10.1007/s00445-014-0796-8.

Lebreiro, S.M., Voelker, A.H.L., Vizcaino, A., Abrantes, F.G., Alt-Epping, U., Jung, S., Thouveny, N., and Gràcia, E., 2009, Sediment instability on the Portuguese continental margin under abrupt glacial climate changes (last 60 kyr): Quaternary Science Reviews, v. 28, no. 27–28, p. 3211–3223, https://doi.org/10.1016/j.quascirev.2009.08.007.

León, R., Somoza, L., Urgeles, R., Medialdea, T., Ferrer, M., Biain, A., García-Crespo, J., Mediato, J.F., Galindo, I., Yepes, J., González, F.J., and Gimenez-Moreno, J., 2017, Multi-event oceanic island landslides: New onshore-offshore insights from El Hierro Island, Canary Archipelago: Marine Geology, v. 393, p. 156–175, https://doi.org/10.1016/j.margeo.2016.07.001.

Leslie, S.C., Moore, G.F., Morgan, J.K., and Hills, D.J., 2002, Seismic stratigraphy of the Frontal Hawaiian Moat: Implications for sedimentary processes at the leading edge of an oceanic hotspot trace: Marine Geology, v. 184, no. 1-2, p. 143–162, https://doi.org/10.1016/S0025-3227(01)00284-5.

Liu, Q., Kneller, B., Fallgatter, C., Valdez Buso, V., and Milana, J.P., 2018, Tabularity of individual turbidite beds controlled by flow efficiency and degree of confinement: Sedimentology, v. 65, no. 7, p. 2368–2387, https://doi.org/10.1111/sed.12470.

Lodato, L., Spampinato, L., Harris, A., Calvari, S., Dehn, J., and Patrick, M., 2007, The morphology and evolution of the Stromboli 2002–2003 lava flow field: An example of a basaltic flow field emplaced on a steep slope: Bulletin of Volcanology, v. 69, p. 661–679, https://doi.org/10.1007/s00445-006-0101-6.

Machado, F., Parsons, W.H., Richards, A.F., and Mulford, J.W., 1962, Capelinhos eruption of Fayal Volcano, Azores, 1957–1958: Journal of Geophysical Research, v. 67, no. 9, p. 3519–3529, https://doi.org/10.1029/JZ067i009p03519.

Madeira, J., and Brum da Silveira, A., 2003, Active tectonics and first paleoseismological results in Faial, Pico and S. Jorge islands (Azores, Portugal): Annals of Geophysics, v. 46, p. 733–761, https://doi.org/10.4401/ag-3453.

Madeira, J., Monge Soares, A.M., Brum Da Silveira, A., and Serralheiro, A., 1995, Radiocarbon dating recent volcanic activity on Faial Island (Azores): Radiocarbon, v. 37, no. 2, p. 139–147, https://doi.org/10.1017/S0033822200030575.

Madeira, J., Brum da Silveira, A., Hipólito, A., and Carmo, R., 2015, Chapter 3 Active tectonics in the central and eastern Azores islands along the Eurasia-Nubia boundary: A review, *in* Gaspar, J.L., Guest, J.E., Duncan, A.M., Barriga, F.J.A.S., and Chester, D.K., eds., Volcanic Geology of São Miguel Island (Azores Archipelago): Geological Society of London, Memoir 44, p. 15–32, https://doi.org/10.1144/M44.3.

Madureira, P., Rosa, C., Marques, A.F., Silva, P., Moreira, M., Hamelin, C., Relvas, J., Lourenço, N., Conceição, P., Pinto de Abreu, M., and Barriga, F.J.A.S., 2017, The 1998–2001 submarine lava balloon eruption at the Serreta ridge (Azores archipelago): Constraints from volcanic facies architecture, isotope geochemistry and magnetic data: Journal of Volcanology and Geothermal Research, v. 329, p. 13–29, https://doi.org/10.1016/j.jvolgeores.2016.11.006.

Masson, D., Le Bas, T., Grevemeyer, I., and Weinrebe, W., 2008, Flank collapse and large-scale landsliding in the Cape Verde Islands, off West Africa: Geochemistry, Geophysics, Geosystems, v. 9, no. 7, 16 p., https://doi.org/10.1029/2008GC001983.

Masson, D.G., Watts, A.B., Gee, M.J.R., Urgeles, R., Mitchell, N.C., and Le Bas, T.P., 2002, Slope failures on the flanks of the western Canary Islands: Earth-Science Reviews, v. 57, p. 1–35, https://doi.org/10.1016/S0012-8252(01)00069-1.

Milkert, D., Alonso, B., Liu, L., Zhao, X., Comas, M., and De Kaenel, E., 1996, 45 Sedimentary facies and depositional history of the Iberia Abyssal Plain, *in* Whitmarsh, R.B., Sawyer, D.S., Klaus, A., and Masson, D.G., eds., 1996 Proceedings of the Ocean Drilling Program, Scientific Results, v. 149, p. 685–704, https://doi.org/10.2973/odp.proc.sr.149.202.1996.

Mitchell, N.C., Beier, C., Rosin, P., Quartau, R., and Tempera, F., 2008, Lava penetrating water: Submarine lava flows around the coasts of Pico Island, Azores: Geochemistry, Geophysics, Geosystems, v. 9, no. 3, https://doi.org/10.1029/2007GC001725.

Mitchell, N.C., Quartau, R., and Madeira, J., 2012, Assessing landslide movements in volcanic islands using near-shore marine geophysical data: South Pico Island, Azores: Bulletin of Volcanology, v. 74, p. 483–496, https://doi.org/10.1007/s00445-011-0541-5.

Mitchell, N.C., Stretch, R., Tempera, F., and Ligi, M., 2018, Volcanism in the Azores: A marine geophysical perspective, *in* Beier, C., and Küppers, U., eds., Volcanoes of the Azores: Active Volcanoes of the World, p. 101–126, Berlin, Heidelberg, Springer, https://doi.org/10.1007/978-3-642-32226-6_7.

Moore, J.G., Normark, W.R., and Holcomb, R.T., 1994, Giant Hawaiian landslides: Annual Review of Earth and Planetary Sciences, v. 22, p. 119–144, https://doi.org/10.1146/annurev.ea.22.050194.001003.

Nakada, M., and Yokose, H., 1992, Ice age as a trigger of active Quaternary volcanism and tectonism: Tectonophysics, v. 212, no. 3–4, p. 321–329, https://doi.org/10.1016/0040-1951(92)90298-K.

Nisbet, E.G., and Piper, D.J.W., 1998, Giant submarine landslides: Nature, v. 392, no. 6674, p. 329–330, https://doi.org/10.1038/32765.

Normandeau, A., Bourgault, D., Neumeier, U., Lajeunesse, P., St-Onge, G., Gostiaux, L., and Chavanne, C., 2020, Storm-induced turbidity currents on a sediment-starved shelf: Insight from direct monitoring and repeat seabed mapping of upslope migrating bedforms: Sedimentology, v. 67, no. 2, p. 1045–1068, https://doi.org/10.1111/sed.12673.

Pacheco, J.M., 2001, Processos associados ao desenvolvimento de erupções vulcânicas hidromagmáticas explosivas na ilha do Faial e sua interpretação numa perspectiva de avaliação do hazard e minimização do risco [Ph.D. thesis]: Universidade dos Açores, Departamento de Geociências, 330 p.

Palacios, D., de Andrés, N., Gómez-Ortiz, A., and García-Ruiz, J.M., 2017, Evidence of glacial activity during the Oldest Dryas in the mountains of Spain, *in* Hughes, P.D., and Woodward, J.C., eds., Quaternary Glaciation in the Mediterranean Mountains: Geological Society of London, Special Publication 433, p. 87–110, https://doi.org/10.1144/SP433.10.

Pimentel, A., Pacheco, J., and Self, S., 2015, The ~1000-years BP explosive eruption of Caldeira Volcano (Faial, Azores): The first stage of incremental caldera formation: Bulletin of Volcanology, v. 77, no. 5, p. 1–26, https://doi.org/10.1007/s00445-015-0930-2.

Pimentel, A., Self, S., Pacheco, J.M., Jeffery, A.J., and Gertisser, R., 2021, Eruption style, emplacement dynamics and geometry of peralkaline ignimbrites: Insights from the Lajes-Angra Ignimbrite Formation, Terceira Island, Azores: Frontiers of Earth Science, v. 9, no. 503, https://doi.org/10.3389/feart.2021.673686.

Piper, D.J.W., Shaw, J., and Skene, K.I., 2007, Stratigraphic and sedimentological evidence for late Wisconsinan sub-glacial outburst floods to Laurentian Fan: Palaeogeography, Palaeoclimatology, Palaeoecology, v. 246, no. 1, p. 101–119, https://doi.org/10.1016/j.palaeo.2006.10.029.

Porcile, G., Bolla Pittaluga, M., Frascati, A., and Sequeiros, O.E., 2020, Typhoon-induced megarips as triggers of turbidity currents offshore tropical river deltas: Communications Earth & Environment, v. 1, no. 1, p. 2, https://doi.org/10.1038/s43247-020-0002-1.

Posamentier, H.W., and Vail, P.R., 1988, Eustatic controls on clastic deposition II—Sequence and systems tract models, *in* Wilgus, C.K., et al., eds., Sea-Level Changes: An Integrated Approach: SEPM (Society for Sedimentary Geology) Special Publication 42, https://doi.org/10.2110/pec.88.01.0125.

Posamentier, H.W., Jervey, M.T., and Vail, P.R., 1988, Eustatic controls on clastic deposition I—Conceptual framework, *in* Wilgus, C.K., et al., eds., Sea-Level Changes: An Integrated Approach: SEPM (Society for Sedimentary Geology) Special Publication 42, https://doi.org/10.2110/pec.88.01.0109.

Povinec, P.P., Litherland, A.E., and von Reden, K.F., 2009, Developments in radiocarbon technologies: From the Libby counter to compound-specific AMS analyses: Radiocarbon, v. 51, no. 1, p. 45–78, https://doi.org/10.1017/S0033822200033701.

Quartau, R., Tempera, F., Mitchell, N.C., Pinheiro, L.M., Duarte, H., Brito, P.O., Bates, C.R., and Monteiro, J.H., 2012, Morphology of Faial Island's shelf: The results of volcanic, erosional, depositional and mass-wasting processes: Geochemistry, Geophysics, Geosystems, v. 13, https://doi.org/10.1029/2011GC003987.

Quartau, R., Hipólito, A., Romagnolii, C., Casalbore, D., Madeira, J., Tempera, F., Roque, C., and Chiocci, F.L., 2014, The morphology of insular shelves as a key for understanding the geological evolution of volcanic islands: Insights from Terceira Island (Azores): Geochemistry, Geophysics, Geosystems, v. 15, no. 5, p. 1801–1826, https://doi.org/10.1002/2014GC005248.

Quartau, R., Madeira, J., Mitchell, N.C., Tempera, F., Silva, P.F., and Brandão, F., 2015, The insular shelves of the Faial-Pico Ridge (Azores archipelago): A morphological record of its evolution: Geochemistry, Geophysics, Geosystems, v. 16, p. 1401–1420, https://doi.org/10.1002/2015GC005733.

Quartau, R., Ramalho, R.S., Madeira, J., Santos, R., Rodrigues, A., Roque, C., Carrara, G., and da Silveira, A.B., 2018, Gravitational, erosional and depositional processes on volcanic ocean islands: Insights from the submarine morphology of Madeira Archipelago: Earth and Planetary Science Letters, v. 482, p. 288–299, https://doi.org/10.1016/j.epsl.2017.11.003.

Ramalho, R.S., Quartau, R., Trenhaile, A.S., Mitchell, N.C., Woodroffe, C.D., and Ávila, S.P., 2013, Coastal evolution on volcanic oceanic islands: A complex interplay between volcanism, erosion, sedimentation, sea-level change and biogenic production: Earth-Science Reviews, v. 127, p. 140–170, https://doi.org/10.1016/j.earscirev.2013.10.007.

Ramsey, C.B., 2008, Deposition models for chronological records: Quaternary Science Reviews, v. 27, no. 1-2, p. 42–60, https://doi.org/10.1016/j.quascirev.2007.01.019.

Reimer, P.J., and Reimer, R.W., 2001, A marine reservoir correction database and on-line interface: Radiocarbon, v. 43, no. 2A, p. 461–463, https://doi.org/10.1017/S0033822200038339.

Reimer, P.J., Austin, W.E.N., Bard, E., Bayliss, A., Blackwell, P.G., Bronk Ramsey, C., Butzin, M., Cheng, H., Edwards, R.L., Friedrich, M., Grootes, P.M., Guilderson, T.P., Hajdas, I., Heaton, T.J., Hogg, A.G., Hughen, K.A., Kromer, B., Manning, S.W., Muscheler, R., Palmer, J.G., Pearson, C., van der Plicht, J., Reimer, R.W., Richards, D.A., Scott, E.M., Southon, J.R., Turney, C.S.M., Wacker, L., Adolphi, F., Büntgen, U., Capano, M., Fahrni, S.M., Fogtmann-Schulz, A., Friedrich, R., Köhler, P., Kudsk, S., Miyake, F., Olsen, J., Reinig, F., Sakamoto, M., Sookdeo, A., and Talamo, S., 2020, The IntCal20 Northern Hemisphere radiocarbon age calibration curve (0–55 cal kBP): Radiocarbon, v. 62, no. 4, p. 725–757, https://doi.org/10.1017/RDC.2020.41.

Romer, R.H.W., Beier, C., Haase, K.M., Klügel, A., and Hamelin, C., 2019, Progressive changes in magma transport at the active Serreta Ridge, Azores: Geochemistry, Geophysics, Geosystems, v. 20, no. 11, p. 5394–5414, https://doi.org/10.1029/2019GC008562.

Ryan, W.B.F., Carbotte, S.M., Coplan, J.O., O'Hara, S., Melkonian, A., Arko, R., Wiessel, R.A., Ferrini, V., Goodwillie, A., Nitsche, F., Bonczkowski, J., and Zemsky, R., 2009, Global

multi-resolution topography synthesis: Geochemistry, Geophysics, Geosystems, v. 10, no. 3, https://doi.org/10.1029/2008GC002332.

Samrock, L.K., Wartho, J.-A., and Hansteen, T.H., 2019, ^{40}Ar-^{39}Ar geochronology of the active phonolitic Cadamosto Seamount, Cape Verde: Lithos, v. 344–345, p. 464–481, https://doi.org/10.1016/j.lithos.2019.07.003.

Satow, C., Gudmundsson, A., Gertisser, R., Ramsey, C.B., Bazargan, M., Pyle, D.M., Wulf, S., Miles, A.J., and Hardiman, M., 2021, Eruptive activity of the Santorini Volcano controlled by sea-level rise and fall: Nature Geoscience, v. 14, no. 8, p. 586–592, https://doi.org/10.1038/s41561-021-00783-4.

Schindlbeck, J.C., Kutterolf, S., Freundt, A., Straub, S.M., Vannucchi, P., and Alvarado, G.E., 2016, Late Cenozoic tephrostratigraphy offshore the southern Central American Volcanic Arc: 2. Implications for magma production rates and subduction erosion: Geochemistry, Geophysics, Geosystems, v. 17, no. 11, p. 4585–4604, https://doi.org/10.1002/2016GC006504.

Schindlbeck, J.C., Kutterolf, S., Freundt, A., Eisele, S., Wang, K.-L., and Frische, M., 2018, Miocene to Holocene marine tephrostratigraphy offshore northern Central America and southern Mexico: Pulsed activity of known volcanic complexes: Geochemistry, Geophysics, Geosystems, v. 19, no. 11, p. 4143–4173, https://doi.org/10.1029/2018GC007832.

Schmidt, C., Hensen, C., Wallmann, K., Liebetrau, V., Tatzel, M., Schurr, S.L., Kutterolf, S., Haffert, L., Geilert, S., Hübscher, C., Lebas, E., Heuser, A., Schmidt, M., Strauss, H., Vogl, J., and Hansteen, T., 2019, Origin of high Mg and SO_4 fluids in sediments of the Terceira Rift, Azores—Indications for caminite dissolution in a waning hydrothermal system: Geochemistry, Geophysics, Geosystems, v. 20, no. 12, p. 6078–6094, https://doi.org/10.1029/2019GC008525.

Schmidt, C., Hensen, C., Hübscher, C., Wallmann, K., Liebetrau, V., Schmidt, M., Kutterolf, S., and Hansteen, T.H., 2020, Geochemical characterization of deep-sea sediments on the Azores Plateau—From diagenesis to hydrothermal activity: Marine Geology, v. 429, https://doi.org/10.1016/j.margeo.2020.106291.

Self, S., 1976, The recent volcanology of Terceira, Azores: Journal of the Geological Society of London, v. 132, p. 645–666, https://doi.org/10.1144/gsjgs.132.6.0645.

Serrano, E., González-Trueba, J.J., Pellitero, R., and Gómez-Lende, M., 2017, Quaternary glacial history of the Cantabrian Mountains of northern Spain: A new synthesis, *in* Hughes, P.D., and Woodward, J.C., eds., Quaternary Glaciation in the Mediterranean Mountains: Geological Society of London, Special Publication 433, p. 55–85, https://doi.org/10.1144/SP433.8.

Sinclair, H.D., and Cowie, P.A., 2003, Basin-floor topography and the scaling of turbidites: The Journal of Geology, v. 111, no. 3, p. 277–299, https://doi.org/10.1086/373969.

Spratt, R.M., and Lisiecki, L.E., 2016, A Late Pleistocene sea level stack: Climate of the Past, v. 12, no. 4, p. 1079–1092, https://doi.org/10.5194/cp-12-1079-2016.

Sulpizio, R., 2005, Three empirical methods for the calculation of distal volume of tephra-fall deposits: Journal of Volcanology and Geothermal Research, v. 145, no. 3–4, p. 315–336, https://doi.org/10.1016/j.jvolgeores.2005.03.001.

Talling, P.J., 2001, On the frequency distribution of turbidite thickness: Sedimentology, v. 48, p. 1297–1329, https://doi.org/10.1046/j.1365-3091.2001.00423.x.

Thomson, J., and Weaver, P.P.E., 1994, An AMS radiocarbon method to determine the emplacement time of recent deep-sea turbidites: Sedimentary Geology, v. 89, no. 1–2, p. 1–7, https://doi.org/10.1016/0037-0738(94)90079-5.

Vlag, P.A., Kruiver, P.P., and Dekkers, M.J., 2004, Evaluating climate change by multivariate statistical techniques on magnetic and chemical properties of marine sediments (Azores region): Palaeogeography, Palaeoclimatology, Palaeoecology, v. 212, no. 1–2, p. 23–44, https://doi.org/10.1016/S0031-0182(04)00302-5.

Vogt, P.R., and Jung, W.Y., 2004, The Terceira Rift as a hyper-slow, hotspot-dominated oblique spreading axis: A comparison with other slow-spreading plate boundaries: Earth and Planetary Science Letters, v. 218, p. 77–90, https://doi.org/10.1016/S0012-821X(03)00627-7.

Walcott, R.I., 1972, Past sea levels, eustasy and deformation of the earth: Quaternary Research, v. 2, no. 1, p. 1–14, https://doi.org/10.1016/0033-5894(72)90001-4.

Walker, G.P.L., 1981, Generation and dispersal of fine ash and dust by volcanic eruptions: Journal of Volcanology and Geothermal Research, v. 11, no. 1, p. 81–92, https://doi.org/10.1016/0377-0273(81)90077-9.

Wallmann, P.C., Mahood, G.A., and Pollard, D.D., 1988, Mechanical models for correlation of ring-fracture eruptions at Pantelleria, Strait of Sicily, with glacial sea-level drawdown: Bulletin of Volcanology, v. 50, no. 5, p. 327–339, https://doi.org/10.1007/BF01073589.

Wall-Palmer, D., Coussens, M., Talling, P.J., Jutzeler, M., Cassidy, M., Marchant, I., Palmer, M.R., Watt, S.F.L., Smart, C.W., Fisher, J.K., Hart, M.B., Fraass, A., Trofimovs, J., Le Friant, A., Ishizuka, O., Adachi, T., Aljahdali, M., Boudon, G., Breitkreuz, C., Endo, D., Fujinawa, A., Hatfield, R., Hornbach, M.J., Kataoka, K., Lafuerza, S., Maeno, F., Manga, M., Martinez-Colon, M., McCanta, M., Morgan, S., Saito, T., Slagle, A.L., Stinton, A.J., Subramanyam, K.S.V., Tamura, Y., Villemant, B., and Wang, F., 2014, Late Pleistocene stratigraphy of IODP Site U1396 and compiled chronology offshore of south and south west Montserrat, Lesser Antilles: Geochemistry, Geophysics, Geosystems, v. 15, no. 7, p. 3000–3020, https://doi.org/10.1002/2014GC005402.

Ward, S.N., and Day, S., 2003, Ritter Island Volcano—lateral collapse and the tsunami of 1888: Geophysical Journal International, v. 154, no. 3, p. 891–902, https://doi.org/10.1046/j.1365-246X.2003.02016.x.

Watts, A.B., Peirce, C., Collier, J., Dalwood, R., Canales, J.P., and Henstock, T.J., 1997, A seismic study of lithospheric flexure in the vicinity of Tenerife, Canary Islands: Earth and Planetary Science Letters, v. 146, p. 431–447, https://doi.org/10.1016/S0012-821X(96)00249-X.

Weaver, P.P.E., and Thomson, J., 1993, Calculating erosion by deep-sea turbidity currents during initiation and flow: Nature, v. 364, p. 136–138, https://doi.org/10.1038/364136a0.

Weston, F.S., 1964, A list of recorded volcanic eruptions in the Azores with brief reports: Boletim do Museu e Laboratorio Mineralógico e Geológico da Faculdade de Ciências, v. 10, p. 3–18.

White, W., Schilling, J.-G., and Hart, S., 1976, Evidence for the Azores mantle plume from strontium isotope geochemistry of the Central North Atlantic: Nature, v. 263, no. 5579, p. 659–663 https://doi.org/10.1038/263659a0.

Wolfe, C.J., McNutt, M.K., and Detrick, R.S., 1994, The Marquesas archipelagic apron: Seismic stratigraphy and implications for volcano growth, mass wasting, and underplating: Journal of Geophysical Research, v. 99, p. 13,591–13,608, https://doi.org/10.1029/94JB00686.

Zanon, V., and Viveiros, F., 2019, A multi-methodological re-evaluation of the volcanic events during the 1580 CE and 1808 eruptions at São Jorge Island (Azores Archipelago, Portugal): Journal of Volcanology and Geothermal Research, v. 373, p. 51–67, https://doi.org/10.1016/j.jvolgeores.2019.01.028.

Zhao, Z., Mitchell, N.C., Quartau, R., Ramalho, R.S., and Rusu, L., 2020, Coastal erosion rates of lava deltas around oceanic islands: Azores Islands Geomorphology, v. 370, https://doi.org/10.1016/j.geomorph.2020.107410.